Palaeogeography, Palaeoclimatology, Palaeoecology 424 (2015) 91–110

Contents lists available at ScienceDirect

Palaeogeography, Palaeoclimatology, Palaeoecology

journal homepage: www.elsevier.com/locate/palaeo

Plant architecture and spatial structure of an early Permian woodland buried by flood waters, Sangre de Cristo Formation, New Mexico

Larry F. Rinehart [a], Spencer G. Lucas [a], Lawrence Tanner [b], W. John Nelson [c], Scott D. Elrick [c], Dan S. Chaney [d], William A. DiMichele [d,*]

[a] New Mexico Museum of Natural History and Science, 1801 Mountain Rd. NW, Albuquerque, NM 87104-1375, USA
[b] Department of Biology, Le Moyne College, Syracuse, NY 13214, USA
[c] Illinois State Geological Survey, 615 E. Peabody Drive, Champaign, IL 61820, USA
[d] Department of Paleobiology, NMNH Smithsonian Institution, Washington, DC 20560, USA

ARTICLE INFO

Article history:
Received 18 September 2014
Received in revised form 5 February 2015
Accepted 8 February 2015
Available online 19 February 2015

Keywords:
Permian
T^0 assemblage
Fossil forest
Self thinning
Dicranophyllum

ABSTRACT

Natural molds of 165 stems were found in life position in a 1 m-thick sandstone bed, lower Permian (Wolfcampian), Sangre de Cristo Formation, northern New Mexico. The sandstone represents a single flood event of a river sourced in the Ancestral Rocky Mountains. Most of the flood-buried plants survived and resumed growth. The stem affinities are uncertain, but they resemble coniferophytic gymnosperms, possibly dicranophylls. Stem diameters (N = 135) vary from 1 to 21 cm, with three strongly overlapping size classes. Modern forest studies predict a monotonically decreasing number (inverse square law) of individuals per size class as diameter increases. This is not seen for fossil stems ≤6 cm diameter, reflecting biases against preservation, exposure, and observation of smaller individuals. Stems ≥6 cm diameter obey the predicted inverse square law of diameter distribution. Height estimates calculated from diameter-to-height relationships of modern gymnosperms yielded heights varying from ~0.9 m to >8 m, mean of ~3 m. Mean stand density is approximately 2 stems/m^2 (20,000 stems/hectare) for all stems >1 cm diameter. For stems >7.5 cm or >10 cm diameter, density is approximately 0.24 stems/m^2 (2400 stems/hectare) and 0.14 stems/m^2 (1400 stems/hectare). Stem spatial distribution is random (Poisson). Mean all-stem nearest-neighbor distance (NND) averages 36 cm. Mean NND between stems >7.5 cm and >10 cm diameter is approximately 1.02 m and 1.36 m. NND increases in approximate isometry with stem diameter, indicating conformation to the same spatial packing rules found in extant forests and other fossil forests of varying ages. Nearest-neighbor distance distribution passes statistical testing for normality, but with positive skew, as often seen in extant NND distributions. The size-frequency distribution of the stems is similar to those of Jurassic, early Tertiary, and extant woodlands; the early Permian woodland distribution line has the same slope, but differs in that the overall size range increases over time (Cope's rule). The early Permian woodland is self-thinning; its volume versus density relationship shows a self-thinning exponent between −1.25 and −1.5, within the range seen in some extant plant stands (−1.21 to −1.7).

Published by Elsevier B.V.

1. Introduction

In situ fossil vegetation provides a direct record of spatial patterns, a class of information that is central to a modern ecological understanding of landscape dynamics (e.g., Legendre and Fortin, 1989; Turner et al., 2001; West et al., 2009). Such fossil assemblages provide a means to study the dynamic aspects of ancient ecosystems, systems that may differ from those of today in such critical ways as species diversity (e.g., Enquist et al., 2007) or the diversity of functional groups (e.g., DiMichele and Phillips, 1996). Preservation of standing vegetation in the fossil record is rare, even more so assemblages that are spatially extensive or have not undergone significant partial deterioration of the least resistant elements. Nonetheless, there are a considerable number of reports of buried upright stems, and these tend to be concentrated in those strata that also are widely exposed by economic activities, such as mining, leading to a somewhat biased distribution in time and space (see Paleozoic summary in DiMichele and Falcon-Lang, 2011). The most desirable of these assemblages for pattern analysis, and its extension thereby to dynamics through the intermediary of ecological theory, are those in which evidence may be adduced for rapid burial of the living stand of plants; the best examples of such cases are ash fall deposits (e.g., Wing et al., 1993; Pfefferkorn and Wang, 2007; Opluštil et al., 2009; Wang et al., 2012), although rapid burial in floods, landslides, or mass movements also can provide an effectively instantaneous record of the spatial organization of original vegetation.

* Corresponding author. Tel.: +1 202 633 1319.
E-mail address: dimichel@si.edu (W.A. DiMichele).

http://dx.doi.org/10.1016/j.palaeo.2015.02.018
0031-0182/Published by Elsevier B.V.

In this paper, we describe 165 fossil stems from the lower Permian (Wolfcampian) interval of the Sangre de Cristo Formation of northern New Mexico (Fig. 1), representing part of a partially buried woodland (Figs. 2–9). We analyze this rare Paleozoic plant stand in terms of its dynamics and ecology, and compare it to younger, Mesozoic and Tertiary "forests" as well as to modern analogues.

2. Materials

2.1. Location, stratigraphy, depositional environment

The fossil vegetation on which this study is based is located in two Bureau of Land Management (BLM) flagstone quarries southwest of San Miguel, New Mexico. The larger of these (Figs. 2A dots on left, 2B–C, 3A), the main, or southeast, quarry, contains the majority of the stem specimens. It is designated New Mexico Museum of Natural History and Science (NMMNH) locality 9082 (National Museum of Natural History locality USNM 43827). Seventeen upright stems of similar character to those at NMMNH locality 9082 also were preserved at an additional quarry, to the northwest of the main quarry (USNM 43829) (Figs. 2A dots on right, 4A). Comparison of the stratigraphic sections at the two sites constrains the fossiliferous beds to the same stratigraphic level, but there is a covered interval between the two quarries. Above both quarries, however, is a distinctive coarse-grained, cross-bedded sandstone containing quartz and feldspar granules that forms a continuous ledge between the two localities. Within the northwest quarry there was evidence of more than one episode of burial, possibly of two plant stands representing successive episodes of colonization of the site following disturbance (Fig. 4).

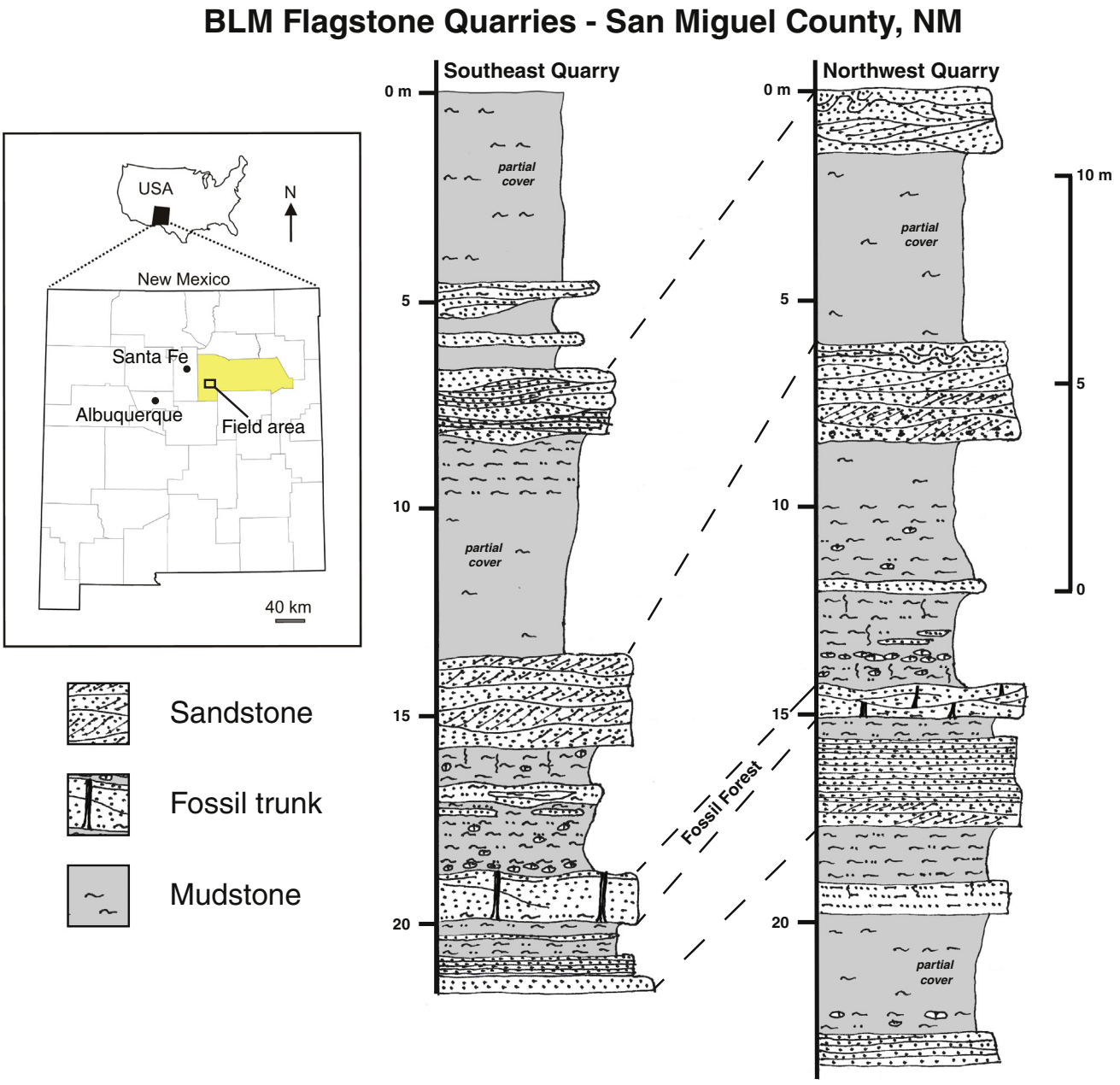

Fig. 1. Sangre de Cristo Formation. Left-to-right: Index map of New Mexico showing the location of the BLM flagstone quarries. Stratigraphic section in the area of the main, Southeast Quarry. Stratigraphic section in the area of the smaller Northwest Quarry. The position of the stem-bearing sandstone beds is noted. The sandstone beds above and below the stem-bearing sandstone interval have been physically correlated between the two exposures.

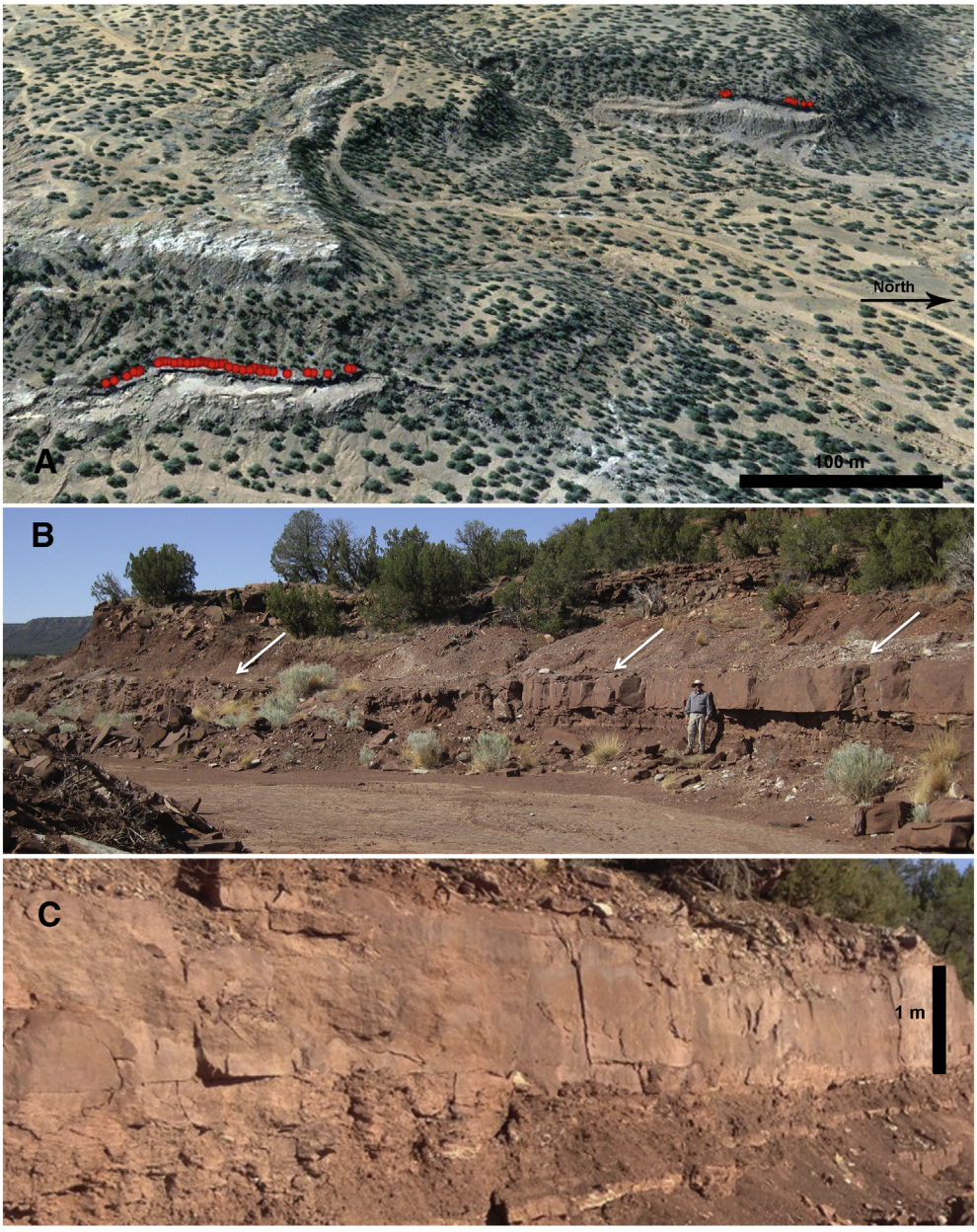

Fig. 2. Stem-bearing Sangre de Cristo Formation outcrops. A. Google Earth screenshot showing the two BLM flagstone quarries comprising NMMNH locality 9082. All data analyzed here were collected at the main, southeast (lower left in image) quarry. The northwest quarry is shown at the upper right. Filled circles mark the location of stems exposed along north–south orientated lines. B. Southern portion of the main quarry (transect sample location) showing the general stratigraphic section. Stem-bearing bed marked by white arrows. Elrick for scale. C. Part of the ~1 m-thick stem-bearing sandstone layer.

Both of these quarries are in the lower Permian interval of the Sangre de Cristo Formation of northeastern New Mexico (Fig. 1). The Sangre de Cristo Formation of the study area represents alluvial fan, fluvial, floodplain, and local shallow lacustrine deposits. These sediments constitute detritus eroded from the nearby Ancestral Rocky Mountains, a series of fault-bounded uplifts that rose episodically throughout Pennsylvanian and into early Permian time (Baltz and Myers, 1999). Much of the Sangre de Cristo Formation is correlative with the Abo Formation of central and southern New Mexico (Lucas et al., 2005, 2012a, 2012b, 2013) and with the lower part of the Hueco Group in southernmost New Mexico (Krainer and Lucas, 1995; Lucas et al., 1998). The Sangre de Cristo Formation represents the piedmont and upper coastal plain surrounding the Ancestral Rockies, whereas the Abo Formation to the south is composed of finer-grained terrestrial clastics deposited on a lower coastal plain. Still farther to the south, the lower Hueco Group consists of shallow-marine carbonates on the margins of the Permian Basin of west Texas. These strata are of Wolfcampian age (Berman et al., 2013), equivalent to the Asselian through early Artinskian, which spans the Coyotean and Seymouran land-vertebrate faunachrons of Lucas (2005, 2006). There is insufficient data in the area of the study outcrops to date the deposit more exactly.

The stem-bearing sandstone bed is in the upper part of a ledge-forming unit that has been traced across several square kilometers. This unit comprises a succession of channel-form sandstone bodies between which are silty mudstones, typically with evidence of at least some pedogenesis (Figs. 1, 2B–C, 3A). Taken as a whole, the unit appears to represent an aggrading alluvial plain. Most of the sandstone is very fine grained, approaching coarse siltstone, and exhibits even, planar bedding, making it suitable for flagstone. Sandstone beds are laterally discontinuous on the scale of hundreds to thousands of meters, grading to poorly exposed, non-fissile red siltstone and mudstone. Locally, small channels (2–3 meters deep, a few tens of meters wide) occur within the

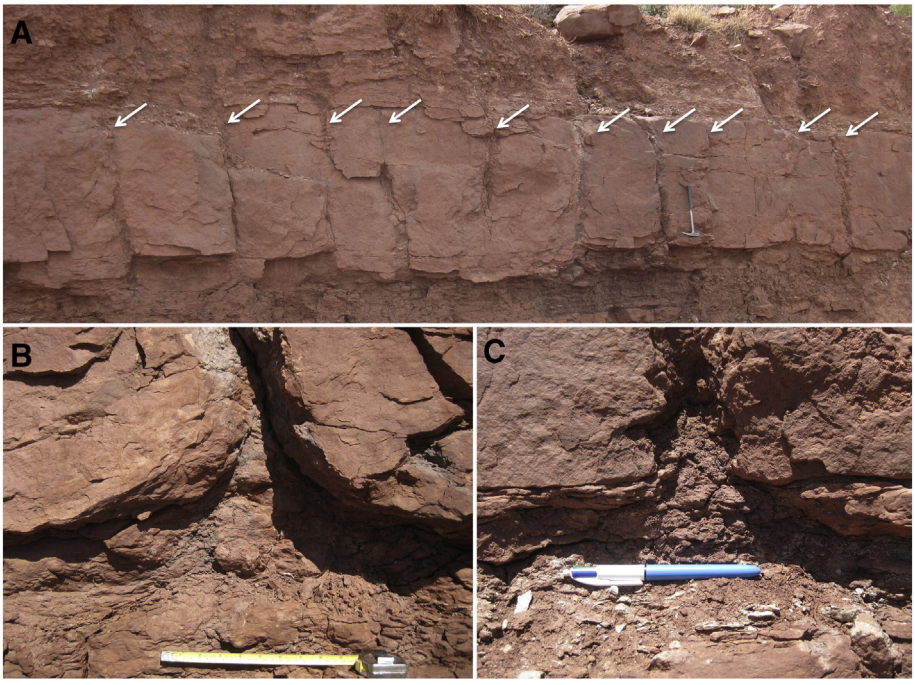

Fig. 3. Natural molds of stems exposed in longitudinal section in the main, Southeast Quarry highwall comprising part of the transect sample. A. Portion of stem-bearing sandstone with 10 stems, marked by white arrows. B. Stem base showing basal flare. Note pedogenic modification of siltstone below the sandstone bed. Scale is 25 cm. C. Stem base showing basal flare. Note pedogeneic modification of siltstone below the sandstone bed. Pen is 14 cm in length.

unit. These small channels contain coarse sand and granules of quartz and fresh pink feldspar, derived from nearby source area of granitic Precambrian rocks in the southern part of the Ancestral Rocky Mountains. They presumably fed a trunk river that lay outside the immediate study area. Flaggy sandstone beds in this unit reveal ripple marks, mud cracks, raindrop impressions, tool marks (formed when a waterborne object such as a piece of wood dragged the bottom), sinuous trails or feeding traces; and the footprints, trackways, and tail-drag marks of small tetrapods. Hunt et al. (1990) described vertebrate trackways and other trace fossils from a site at the same stratigraphic level as ours, less than 1 kilometer south of the quarries where the present study was made.

Several lines of evidence demonstrate that the features described herein are, in fact, the molds of stems/trunks of early Permian vegetation. Alternate interpretations of these features, as dewatering pipes, for example, are not supported by the points enumerated below, expanded upon elsewhere in the text. Dewatering features are not known to form bifurcating structures or to host calcrete, and commonly display internal structure of disrupted lamination (Buck and Goldring, 2003; Odier et al., 2006; Sherry et al., 2012). Neither do the features we describe conform to the characteristics of clastic dikes in their shape, density, or lack of a clastic filling (e.g., Nelson et al., 2013).

(1) All observations are consistent with the generalization that the features are approximately vertically oriented cylinders. The features are observed mainly in vertical longitudinal-section, rather than plan-view, but even in longitudinal-section, the curvature of the walls visible in the vast majority of the features makes it clear that they are cylindrical in form, not tabular. This can be observed in Fig. 9A (block surface photo). Although the circular nature of most of the circled features on the surface is partially obscured by their nodular carbonate infilling, the stem molds on the edges of the block, from which the carbonate has been removed, show that they are almost perfectly cylindrical. Please note the mold marked "6.5" (its diameter in centimeters), halfway down the right side of the photo. Also note the feature marked "2.5" at the top of the block, and the one marked "3.0" on the upper left side of the block. All are half-circles, reflecting the intersection of these weak points by the joints that form the block boundaries. As we discuss below, the joints preferentially intersect the stem molds near their true diameter. Thus, they are not fissure fills.

(2) Many, although not all of the cylinders are surrounded by a drab halo formed by the reduction of Fe-oxides in the enclosing sediments. This is consistent with an original organic core that decayed after burial.

(3) The structures bear a number of features consistent with a biological origin and not with formation by the upward movement of water or sediment from beneath the sandstone layer. For example, many bifurcate downward, with smaller branches split off laterally at a descending angle, typical of adventitious roots. Tubes $\leq$6 cm in diameter are not vertical, but rather lean to the south (in all the cases we observed) at various angles. In all of the specimens in which it could be observed, the bottom is distinctly bell-shaped, widening downward, and in many of the specimens there were distinct rhizoliths emanating from the base.

(4) Structurally the cylinders consist of a firm outer wall that separates the host sedimentary rock from a filling consisting largely of nodular calcrete.

The stems are most abundant in an approximately one-meter-thick sandstone bed that is distinguishable from other sandstone beds in the area by its crossbedding, lithology, and thickness (Fig. 2B white arrows, 2C). This bed has a tabular, sheet-like geometry and sedimentary structures, mainly planar crossbeds and climbing ripple sets, indicative of rapid deposition by traction currents under varying flow conditions. There is no evidence of a significant pause in deposition or exposure during deposition. The stem-bearing sandstone is underlain by a dark red, carbonate-rich, muddy, sandstone/siltstone with a pedogenic overprint (Figs. 2B; 3A–C, 4A–C, 5A–C). Drab root traces and occasional rhizoliths and calcrete nodules occur in this layer, directly under individual fossil stems (Figs. 3B–C, 4B–C, 5A–C). Small exposures of the

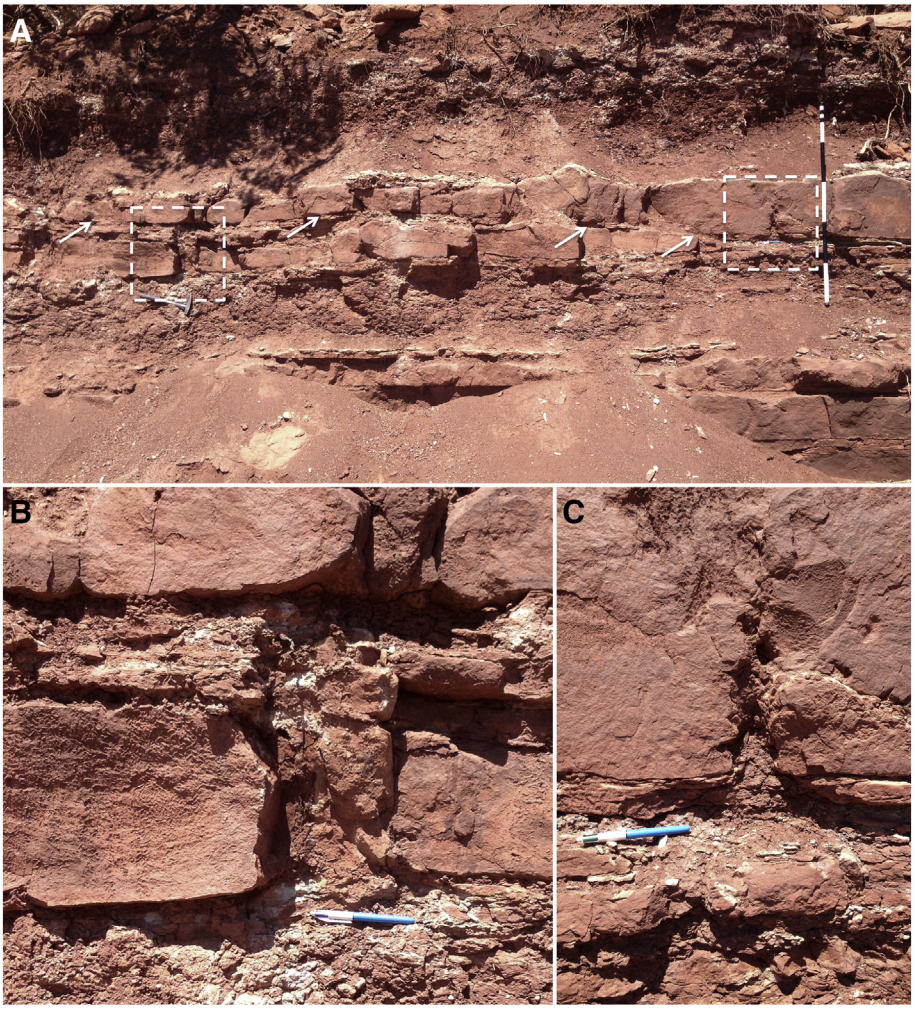

Fig. 4. Northwest Quarry, stem-bearing Sangre de Cristo Formation outcrop. A. Double sandstone bench, separated by erosional contact (white arrows). The lower bench is overlain by a siltstone that has been completely removed by erosion on the right side of the contact. Stem molds occur in both sandstone benches; examples marked by white, dashed-line boxes, enlarged below. Staff = 1.5 m (ruled in feet, with upper ½ foot divided in tenths of feet). B. Stem mold from right side in image A, buried by lower sandstone layer. Note flared base rooted in underlying siltstone, projection of stem into the overlying siltstone and truncation by second sandstone layer. Pen = 14.5 cm. C. Stem mold from left side in image A, buried by upper sandstone layer. Note flared base rooted in erosional remnant of underlying sandstone, the top of which is slightly altered by pedogenesis. Pen = 14.5 cm.

top of the sandstone bed show rectangular joint sets. These comprise generally longer, north–south oriented joints that are intersected by shorter, perpendicular, east–west trending joints.

The stems appear to have been entombed by flood-borne, fine sand that was deposited on a soil surface in which the stems were rooted. The fossil stems themselves are natural molds in the sandstone (Figs. 3A, 4B–C, 5A–C), and most are partially to completely in-filled with greenish-gray carbonate that typically has a nodular to knobby texture (Fig. 5A, C–D), although less commonly is layered parallel to the walls of the mold (Fig. 5B). Where visible, the stems show a basal flare just above the point where they were originally rooted (Figs. 3B–C; 4B–C, 5A–C). On top of much of the stem-bearing sandstone, carbonate nodules, similar to those filling the stem molds, occur in a layer that can be up to a few cm thick and above which is a siltstone with a pedogenic overprint (Fig. 3A). Where preservation is exceptionally good, the stems can be seen to have projected into these superjacent layers (Figs. 4A, 8A). Lateral to many of the stem molds both downwardly directed and upwardly directed lateral appendages are present (Figs. 5B, 6). We infer the downwardly directed axes to be roots, indicating adventitious rooting into the entombing sandstone following burial; the upwardly directed axes appear to be lateral shoots that also may have been initiated in response to burial in flood sediments. All of the larger stems (generally ≥6 cm diameter) are vertically, or nearly vertically disposed (Figs. 3A, 4–6). Many of the smaller stems are inclined to the south, typically 30° to 40°, but some as much as 60° or more (Fig. 7). Based on some of the data presented below, many of the smallest individuals were probably completely flattened by the inundation and thus removed from the statistical sample.

2.2. Preservation and identity of the plants

The fossils, as noted above, are preserved as molds of standing buried stems, which later decayed, leaving hollow tubes in both the entombing sandstone and in the basal portions of the overlying sediment (Figs. 3–7). Stem bases, where exposed, are flared and show evidence of rooting in the paleosol beneath the flood-deposited sandstone (Figs. 3B–C, 4B–C, 5A–C, 6), deduced from the presence of rhizoliths extending outward into the paleosol from these flared stem bases. The molds are partially filled with ropy to nodular, brecciated carbonate (Figs. 3–6).

Evidence suggests that the plants were not killed by burial, thus the formation of the molds occurred some time afterward. This is indicated by several features: (1) The laterally to downwardly directed appendages that were found on many stems (Figs. 5B, 6B, 7B). These originated at multiple, irregularly spaced levels from the sides of the stem molds, and any one stem could show the presence of these features at multiple

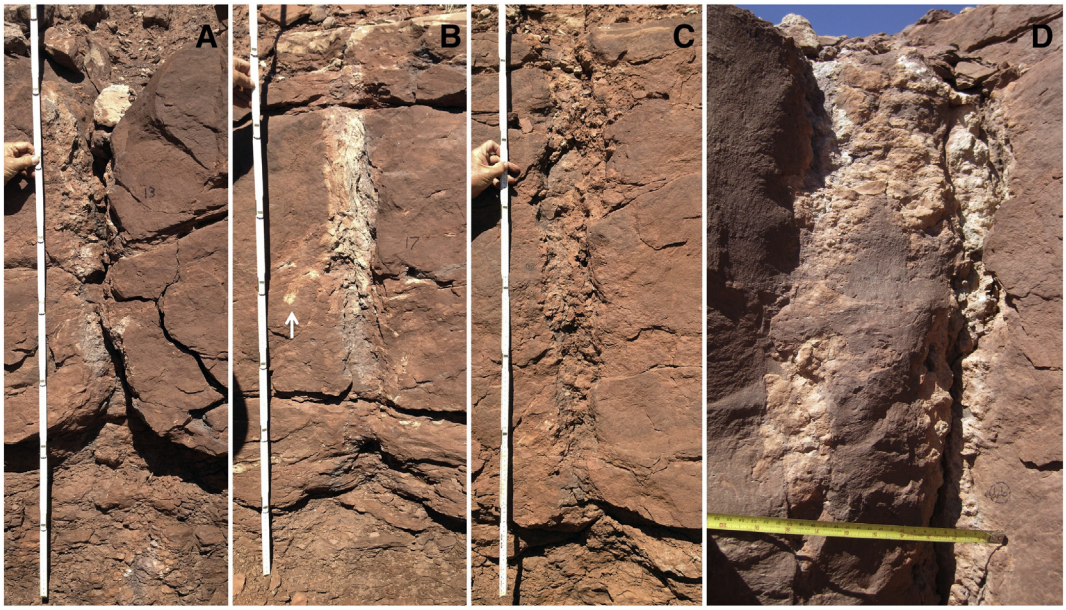

Fig. 5. Natural molds of stems exposed in longitudinal section in the quarry highwall comprising part of the transect sample. Numbers assigned to stems are as listed in Appendix I. Photographs A-C are shown at the same magnification. A. Number 13, 11.5 cm diameter. Most of the carbonate infilling has fallen out of this specimen. The small, light-colored spots directly under the basal flare of the tree are bits of rhizoliths. B. Number 17, 7.5 cm diameter. Carbonate infilling is particularly dense in this specimen. C. Number 35, 9 cm diameter, showing loose carbonate infilling. D. Number 66, 22.5 cm in diameter, filled with nodular carbonate. Scale in cm (27) and inches (10.5).

levels. The appendages appear to be the remains of roots. They most likely indicate that the plants rooted into the sediment after burial. In one instance a large root-like feature was noted that had the characteristics of a prop-root, but in general, root-like lateral appendages were not strongly downwardly directed nor found to extend from the main stems to the subjacent soil. (2) Upwardly directed lateral appendages are present on many of the stems (Fig. 6). These are less than half the diameter of the parent axes and may themselves bear lateral appendages that are, again, proportionally smaller than the axes that bear them (Fig. 6). These originate at multiple, irregularly spaced, distances from the stem bases and also may bear root-like appendages (Fig. 6C). These most closely resemble lateral, adventitious branches, presumably formed after burial of the parent axes. In some cases, these lateral branches may have been present prior to burial – in such instances the branch departs at nearly right angles to the parent axis and then turns sharply upward. (3) Some of the stems were observed to extend upward into the overlying sediment (Figs. 4B, 8A), which rests with a sharp disconformity surface on the sandstone in which the stems are entombed. This indicates that the stems had not decayed, leaving mold cavities, when this later sediment was deposited. The decay that created the hollow areas in the sandstone occurred sometime after both a hiatus of indeterminate duration and deposition of later sediment. (4) The carbonate filling of the stem molds is geochemically similar to carbonates in the overlying, pedogenically altered siltstone, which suggests that the two carbonate deposits formed under similar conditions.

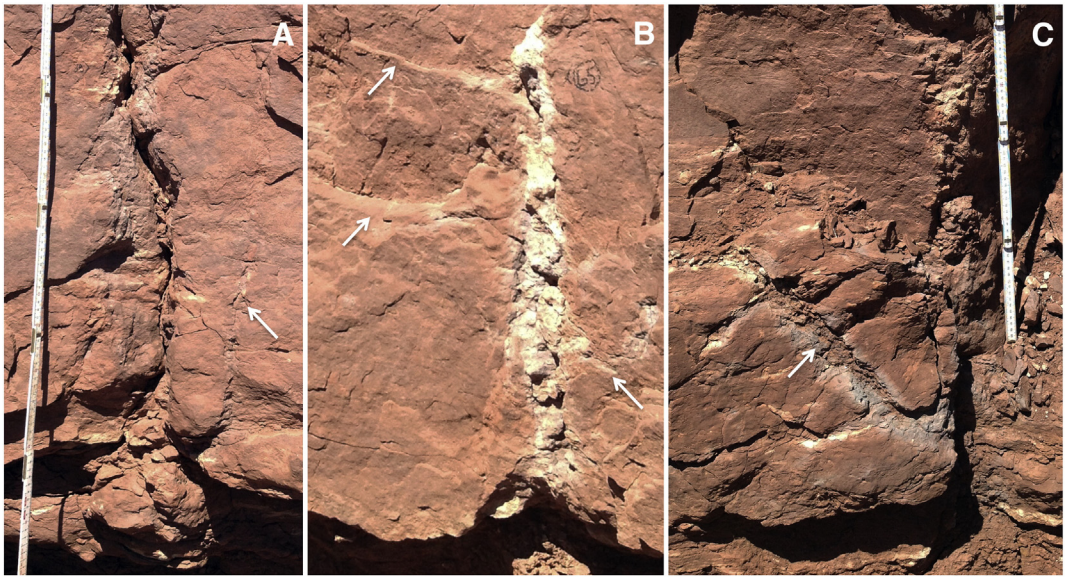

Fig. 6. Natural molds of stems exposed in longitudinal section in the quarry highwall comprising part of the transect sample, illustrating roots and shoots originating from the buried portion of the stems. Numbers assigned to stems are as listed in Appendix I. Photographs are shown at the same magnification. A. A shoot (arrow) originating at the base of stem number 38 and extending more than 40 cm vertically. B. Lareral roots (arrows) originating approximately 30 cm above the base of stem number 65. C. A shoot with lateral branching (arrow), originating above the base of stem number 109 and extending more than 30 cm. Scale divided into 10 cm increments (dark lines).

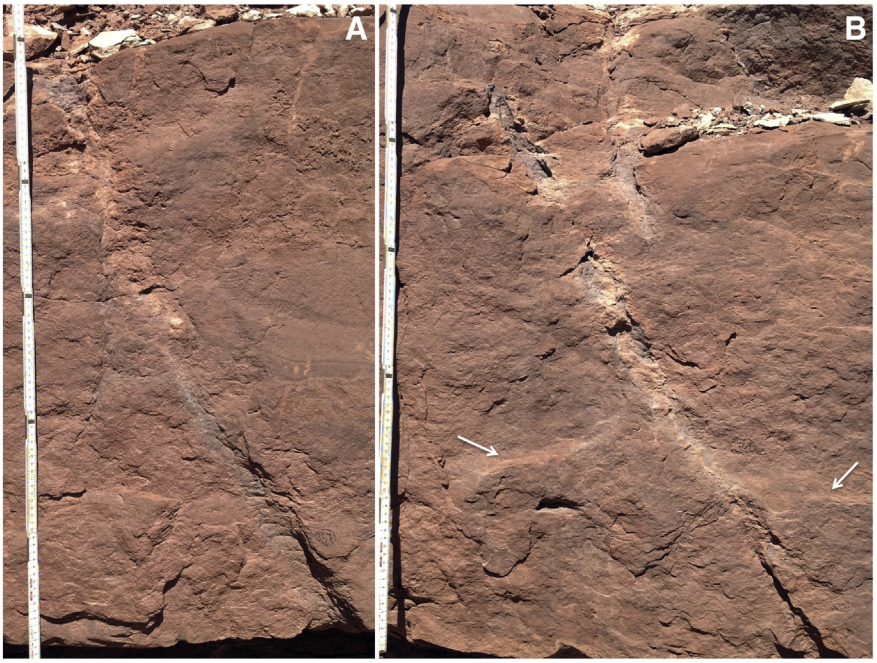

Fig. 7. Natural molds of small, leaning stems exposed in longitudinal section in the quarry highwall comprising part of the transect sample. Numbers assigned to stems are as listed in Appendix I. Photographs are shown at the same magnification. A. Number 57, 4 cm in diameter. Inclined 35° to the south. B. Number 63, diameter 3.5 cm. Inclined 30° to the south. Scale A–E: ~16 cm between visible joints in folding ruler.

The taxonomic identity of the stems is uncertain. There is no strong indication that more than one species is represented given the consistency of architecture and the nature of taphonomic preservation; however, distinct size classes are present in the sample that could represent mixed species. A possible indication that the stand is a species mixture comes from the deflection of small diameter stems from a strictly vertical disposition in the entombing sediment (Fig. 7). However, all stems appear to have had the capacity to recover from burial, all have similar rooting bases, and both lateral roots and lateral shoots were present in all size classes. Poorly preserved foliage-bearing branches similar to those of walchian conifers (Fig. 8E), small branches with possible attached foliage similar to that of the coniferophyte *Dicranophyllum* (Fig. 8B) and a single septate-pith specimen (*Artisia* Sternberg 1838) (Fig. 8D) attributable to the coniferophytes were found in association with the stem molds, but on isolated blocks of sandstone (e.g., Fig. 2B). The *Artisia* specimen is typical of cordaitalean gymnosperms, a group best known from the Pennsylvanian but extending into the early Permian (Mamay, 1967). Septate piths, however, also have been identified in walchian conifers and dicranophylls (Renault and Zeiller, 1888; Hernandez-Castillo et al., 2009; Falcon-Lang et al., 2011), and may have been typical of primitive coniferophytes generally.

None of the stem molds showed clear, taxonomically diagnostic surface texture, even after removal of the carbonate infilling. A single specimen (Fig. 8B–C), found in an isolated block in the northwest quarry, gave weak indication of a regular diamond-shaped surface pattern, perhaps of leaf bases, similar to that found on some plants, such as *Dicranophyllum*.

In terms of gross morphology, the features of the stems permit us to rule out certain taxonomic affinities more readily than they indicate a particular identity. Calamitaleans, which are an initial suspect, given the location of the plants in an environment subject to repeated flooding and sediment inundation, are largely ruled out by the irregular placement of lateral appendages; the modular node-internode construction of the calamitaleans should lead to a regular whorled disposition of appendages, and is diagnostic of that group. In addition, the bell-shaped base and central rooting are not characteristic of most calamitaleans, and the surface texture of the stems, lacking clear node-internode architecture or longitudinal ribbing, is similarly uncharacteristic. Isoetalean lycopids, particularly the cormose-based forms similar to *Chaloneria* or *Pleuromeia*, appear to be unlikely candidates in light of the lack of isoetalean rooting systems, the indications of adventitious rooting, and the branching architecture, particularly if those branches developed post-burial. Neither do the stems have features that might be expected of marattialean tree ferns – evidence of a rugose outer surface of irregular elongate ridges, created by a root mantle, or the presence of attached leaf bases or scars. In addition, marattialeans are not known to produce the kinds of localized lateral roots and shoots found in these specimens.

Seed plants are the most likely Paleozoic candidates for stem affinity. The medullosan pteridosperms and their allies, the callipterids, remain a remote possibility. The size, rooting and lateral appendages are consistent with medullosans, sensu lato, although lateral branches, particularly if secondarily initiated following burial, are not typical of the genus *Medullosa* itself, at least as far as it is known at present. Little is known about callipterid gross morphology, although callipterids appear to be derived from medullosan ancestors.

More likely among the seed plants is a coniferophyte affinity. This group includes the conifers, cordaitaleans and dicranophylls. Perhaps the least likely are the woody walchian conifers, despite the presence of several walchian-conifer branch specimens in sandstone blocks within the quarry (Fig. 8E). Walchians, as far as they are understood, had stereotypical growth architectures that do not include lateral branches of the kind found in attachment to the upright stems; the plagiotropic habit of walchians (Looy, 2013) is accompanied by branch scars or a regular disposition of lateral branches, often in pseudowhorls, which is not evident in the stem molds. Alternatively, the growth architecture of the stem molds is consistent with orthotropic growth habits typical of voltzian-voltzialean conifers (Looy, 2007); a recent discovery of these plants in lower Permian deposits (Falcon-Lang et al., submitted for publication) leaves open the possibility of such an identity. Similarly, the growth architecture of the coniferophyte *Dicranophyllum*, which was an unbranched, leafy

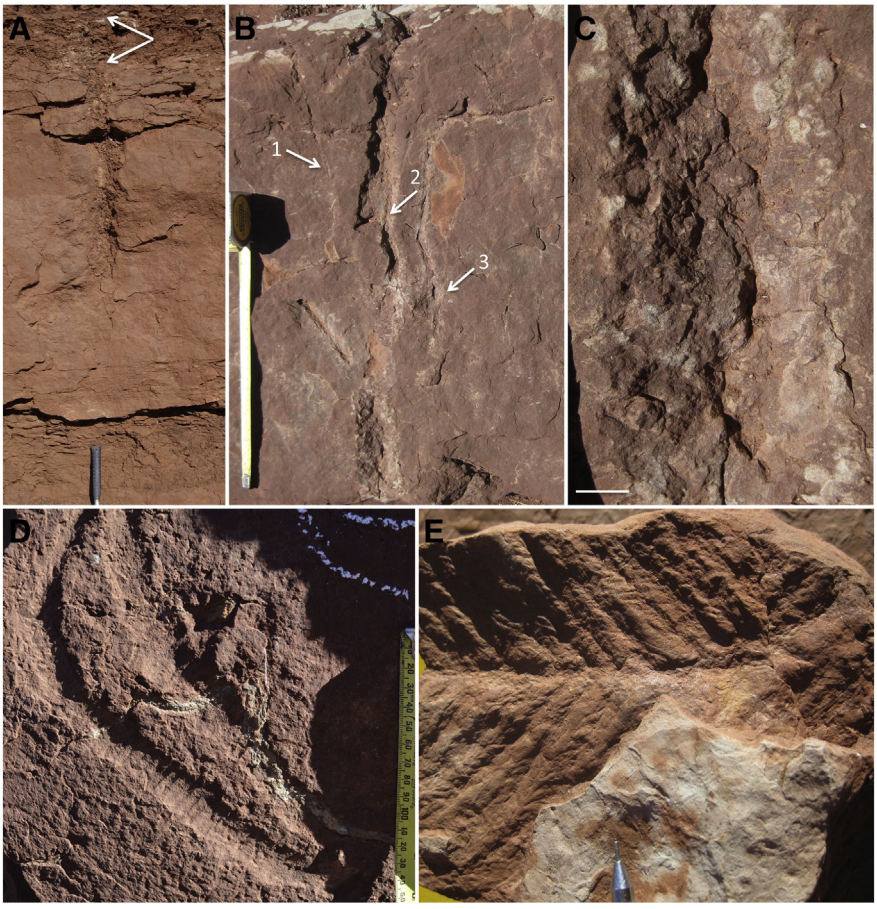

Fig. 8. Details of selected plant impressions. A. Upper portion of a stem projecting into the sediment overlying the transect-sample sandstone bed. Portion above the top of the sandstone is marked by white arrows. Geological hammer handle at base for scale. B. Stem from lower quarry, fallen block, with attached lateral appendages, possibly leaves, marked by numbered arrows, and surface impression (enlarged in image 7C). Lateral appendages 1 and 2 are straight, thin, and similar to the bases of *Dicranophyllum* leaves; appendage 3 is possibly a lateral branch but could be a leaf, forked in its upper portion. Exposed portion of measuring tape is 25 cm. C. Surface features of stem in 7B. Note vague but consistent diamond-shaped surface patterns, perhaps leaf bases similar to those found on *Dicranophyllum*. Scale bar = 1 cm. D. An impression of *Artisia*, a pith cast, in fallen block number 27. Scale bar = 2 cm. E. Impression of walchian conifer branch from fallen black in transect-sample quarry. Tip of mechanical pencil at base for scale. USNM specimen 610504.

pole, does not conform in detail to that of the stem molds, but remains within the realm of possibility.

Dicranophyllous plants are centrally rooted with straight, slender trunks and a characteristic pattern of diamond-shaped leaf scars densely packed on the stem surface (Barthel et al., 1998; Barthel and Knoll, 1999; see also Kerp et al., 2007). Leaf-like appendages were found in association with one stem cast from the northwest quarry that also had vaguely diamond-shaped markings on the outer surface of the stem (Fig. 8B, appendages 1 and 2 in particular). The leaf-like structures were thin and stiff, but could not be ascertained unquestionably to be leaves. Although forking was not observed, they are consistent, as far as preserved, with the leaves of a *Dicranophyllum* species such as *D. hallei*, which are quite long and forked only in their terminal regions (Barthel and Noll, 1999). An impression of *Artisia* Sternberg 1838 (Fig. 8D), a septate pith cast of coniferalean affinity, also was found in association with the stems. This type of pith is most commonly attributed to cordaitaleans (Chamberlain, 1966; Tidwell, 1975), an order best known from the Carboniferous, but ranging into the early Permian (Mamay, 1967). However, septate piths also have been described from walchian conifers (Hernandez-Castillo et al., 2009; Falcon-Lang et al., 2011) and *Dicranophyllum* (Renault and Zeiller, 1888).

When the various lines of evidence are taken into consideration, taxonomic identification of the stem molds must remain equivocal. The closest similarity appears to be with the coniferophyte *Dicranophyllum*, which is known to occur, though rarely, in correlative red beds of the Abo Formation (DiMichele et al., 2013), and thus in strata age-equivalent and environmentally similar to the red beds of the Sangre de Cristo Formation (Lucas et al., 2013). However, similarity to pteridosperms cannot be ruled out, nor can affinity with an unknown group of plants or a partially known group (among the many known only from foliage) for which the growth architecture is not known.

3. Methods

3.1. Sampling

Two distinct measurement samples, encompassing a total of 165 stems, were acquired at NMMNH locality 9082, the main, southeast quarry. These are referred to as the "transect sample" (Fig. 3A) and the "surface sample" (Fig. 9A). A total of 135 stem diameters were measured from these samples; 77 in the transect sample (Appendix I) and 58 in the surface sample (Appendix III). Other measurements acquired are described below. Statistical analyses of spatial distribution were carried out on these two samples. Statistical analysis was performed using JMP 10.0.0 (2012), and PAST (Hammer et al., 2001) statistical-analysis software.

3.1.1. Transect sample

One hundred and ten stems were identified and measured along a 158 m-long north–south-trending transect. The stems are exposed in longitudinal section in life position in the quarry highwall (Fig. 3A, white arrows). These data comprise the "transect sample," although

Fig. 9. Fallen blocks of the stem-bearing sandstone comprising part of the surface sample. A. The clean, top surface of block number one, 1.3 m long, 0.7 m wide. An especially dense block of ~0.9 m^2 area, containing 10 tree stems varying from 1.5 cm to 10 cm in diameter (marked in chalk); B. The top surface of block number 15, 0.8 m long, 0.3 m wide, 0.32 m^2 area with heavy carbonate coating which probably obscures some small stems. Note stick impressions. Scale bar = 0.5 m.

they are, in the strict sense, neither a line transect sample, nor a line intercept sample; we discuss this below.

Measurements were made of distance to next stem, proceeding from north to south along the quarry highwall, and of stem diameter (Appendix I). Stem diameters were measured, as nearly as possible, at a point 0.5 m above the basal flare of each stem mold (near the center of the fossil-bearing sandstone bed). The typical "breast-height" (1.37 m) measurements of forestry studies were not possible because the preserved stems all terminated at ~ 1 m height. If the stems were clearly not round or varied considerably in diameter, two or three measurements were taken in the vicinity of 0.5 m above the basal flare and averaged. In cases where the true diameter of the tree was not revealed (i.e., if the stem impression and/or carbonate infilling was shallow and clearly not a half-circle) no measurement was made. In all, 77 diameter measurements of reasonable quality were collected from the 110 specimens present on the outcrop.

During measurement a question arose regarding whether the large, vertical joint surface that forms the east-facing quarry wall preferentially intercepted the stems so as to reveal their true diameter. Given the density of the stem molds, it seemed possible that they could have created zones of weakness along which a joint surface could propagate. Alternatively, it had to be considered that the joint surface intercepted the stem molds randomly, only rarely showing the true diameter and more often showing some fraction of that diameter. After several visits to the outcrop, and after taking measurements and making observations on both the joint face and the upper surface of the sandstone bed, it seems likely that the rock most often fractured through the center of the stems preferentially, so as to reveal the true stem diameters. This preferential fracture can be attributed to a field enhancement effect that determines how stress is distributed and concentrated around a hole in a rock slab. The stress field concentrates around a circular hole in a slab under tension so that it is maximized perpendicular to the applied tensional stress and at the full diameter of the hole (Fig. 10A) (Long et al., 1996). Thus, fractures originating at or intercepting such a hole would preferentially propagate in this enhanced stress zone and would most likely reveal the full diameter.

The basically north–south-trending joint surface that exposes the stems of the transect sample actually contains numerous slight, or occasionally severe (up to 90°), east or west jogs that formed as the propagating joint changed direction to intercept stems near its path. This pattern strongly supports the idea that stress field enhancement around the holes in the sandstone controlled the path of the propagating joint that formed the exposure surface.

Our transect sample data cannot be treated as a line transect sample in the strict sense, because a true line transect must have finite width for the purpose of density calculations (Anderson et al., 1979; Burnham et al., 1980). The NMMNH locality 9082 transect data are practically one-dimensional, lacking any well-defined width. Nor can they be treated as line intercept data because line intercept data must be taken along straight-line segments that are not influenced by the presence or absence of an event (stem) (e.g., Anderson et al., 1979; Gregorie and Valentine, 2003; Salo et al., 2008). The events at NMMNH locality 9082 are exposed along a line that jogs from one stem to the next, clearly under the influence of the next stem near its path.

3.1.2. Surface sample

Fifty-five stems contained in fallen blocks of the stem-bearing sandstone were measured. These data together with data from the small *in situ* exposure of the top of the sandstone layer are called the "surface sample" (Fig. 9). Ideally, the best data would have been obtained by clearing off the top of the stem-bearing sandstone

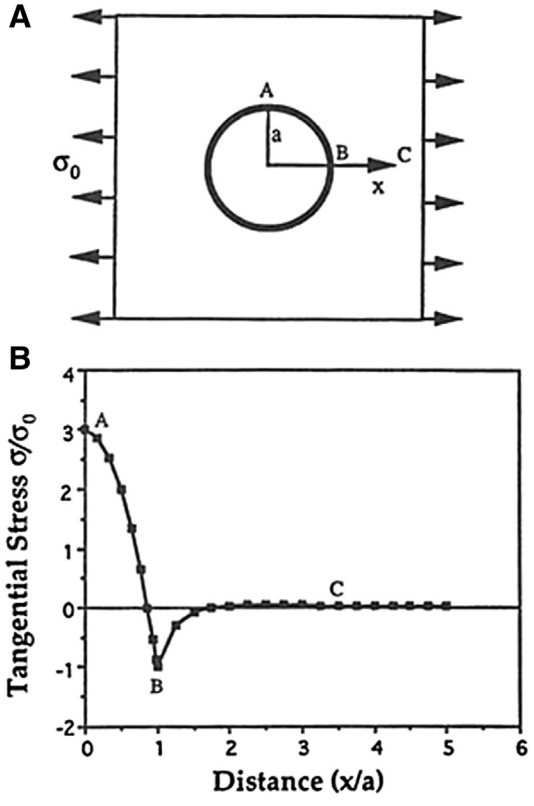

Fig. 10. A. Diagram showing a hole in a rock slab under tension. B. Plot of tangential stress versus distance showing that stress is enhanced and concentrates at the maximum diameter of the hole, perpendicular to the applied stress. Stress is graphed for only 1/4 of the hole because symmetry is assumed (From: Long et al., 1996; p. 36, Fig. 2.5).

and mapping the stems in their two dimensional positions (e.g., Hayek and Buzas, 1997, Fig. 1.2; Pole, 1999, Fig. 10). Because of the generally thick, indurated overburden, this approach was impractical except in very small areas where the overburden was thin. One such small area (~three m^2) was cleared and mapped and will be described below as the *in situ* sample (Fig. 11A). This sample contained three stems within its borders and seven stems along its edges (already counted in the transect sample). Most of the surface data were acquired from fallen blocks of the stem-bearing sandstone. Several of these blocks were directly under the outcrop from which they had fallen; numerous others had been pushed out of the quarry so that their original position could not be ascertained.

Thirty-six fallen blocks of the stem-bearing sandstone were identified and measured. Block area and number of stems (Appendix II) and stem diameter (Appendix III) were recorded. To enable more accurate density and distribution calculations, all positively identifiable blocks of the stem-bearing sandstone were measured for area whether they contained stems or not. Block surface areas varied from 0.3 to 2.4 m^2, and the number of stems per block varied from zero to 10 (Fig. 9A). In some cases, the surface of a block was almost completely obscured by a heavy coating of carbonate similar to the infilling of the natural stem molds (Fig. 9B). This coating, no doubt, resulted in the loss of some data, particularly with respect to the smaller stems.

Stems in the fallen blocks are exposed as if viewed from above or below, depending on the orientation of the fallen block. Crossbedding set relationships in the sandstone were used to identify their original upright orientation. Diameters were measured well above the basal flare of the specimens. Their two dimensional location on the upper surface of the stem-bearing sandstone was thus revealed and recorded.

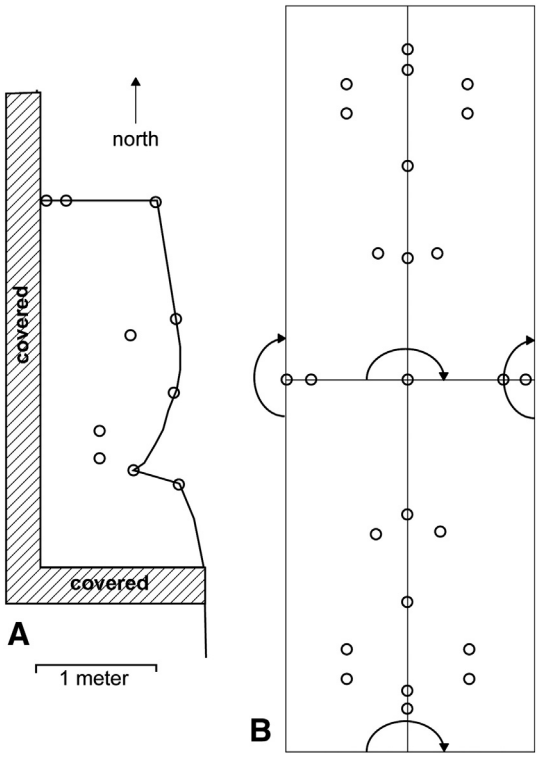

Fig. 11. Schematic diagram of the *in situ* sample. A. Map of a one meter-wide by three meter-long area excavated west of the generally north–south trending transect line. Small circles represent the location of stems. Note that most stems are along the edges of the sample. B. Edge effects were negated by mirror imaging (arrows) the *in situ* sample area (lower left); first to the east and then to the north. Edges were straightened and squared for simplicity.

3.2. Statistics: measurement and analysis methods

3.2.1. Stem height estimation

Stem diameters were measured in the field and are tabulated (Appendix I). We used an allometric relationship based on the power equation of Niklas (1994) to calculate estimates of stem height (H):

$$H = \beta D^{\alpha}$$

in which β is a scaling coefficient (=0.792), D is the diameter, and α is the allometric constant (=0.723 for dicot and gymnosperm trees). Williams et al. (2003a, 2003b) also have proposed a means to estimate tree heights. We choose to use the Niklas height formula, however, rather than that of Williams et al. because the former is based on many dicot and gymnospermous tree species (N = 56), whereas the Williams et al. formula is specific to a single species of very tall, slender tree, the conifer *Metasequoia glyptostrobides*.

3.2.2. Density

Mean density was estimated by three methods: (1) Using the surface sample data (Appendix II), we find that the sum of the fallen block surface areas equals 29.45 m^2. Fifty-five stems are contained within this area. However, many of the stems (38%) in the surface sample occur on the edges of the fallen blocks because the stem molds themselves influenced the propagation of the joints that formed the blocks. Edge effects, where an "event" falls on the edge of a study area, are problematic (Hayek and Buzas, 1997; Dixon, 2012). In the case of the surface data, the edge effects can cause an underestimate of the area and thus an overestimate of density.

(2) A second density estimate, albeit over a very small area, is provided by the *in situ* sample, a one-meter by three-meter area where the overburden was manually removed from the tree-bearing sandstone to expose the fossils from above (Fig. 9). From the *in situ* area map (Fig. 11A), it is clear that most of the stems are located on the transect line, at the northern and eastern edges of the area. To negate the edge effects, we assumed that the stems were distributed to the east and west as they were along the north–south transit line, then we mirror imaged the approximately rectangular *in situ* area, first to the east, and then to the north (Fig. 11B), creating a new rectangular area, four times larger, in which the stems were not located along the edges. The result of this approximation was 25 stems in a 12 m^2 area.

(3) Density of the tree-sized stems was estimated using the forestry definition of a "tree" as stems having a breast-height diameter >7.5 cm or, in some cases, >10 cm; stems having smaller diameters are considered undergrowth (Pole, 1999). In previous studies of fossil forests (Jefferson, 1982; Mosbrugger et al., 1994; Pole, 1999), workers sometimes recorded all stems >1 cm diameter, but only counted these as trees if they fit the forestry definition of a tree in terms of diameter. In order to provide density data that are more directly comparable to those of modern forest stands, we also calculated density when only stems with diameters of >7.5 cm and >10 cm are counted. We note that the density calculations for the >7.5 cm and >10 cm diameter stems must be considered very approximate due to small sample size (>7.5 cm, N = 7; >10 cm, N = 4).

3.2.3. Spatial distribution pattern

The spatial distribution of plants over an area varies from clumped or aggregated, to random, to ordered (as in an orchard). Aggregation may indicate a clumped distribution of resources (e.g., light, nutrients, or water) or interdependencies (e.g., support or defense), whereas a uniform distribution may indicate competition for resources among individuals (Tilman, 1988).

A random distribution of events over an area or along a straight line is described by the Poisson distribution. Therefore, a Poisson distribution of a spatial data set may be taken as evidence of its random distribution. The equivalence of the mean and variance is a unique

characteristic of the Poisson distribution and may be used as a test for its presence in a data set. In plant distribution data such a test may be performed by plotting the log-transformed mean versus the log-transformed variance of the number of plants within quadrats of varying size (Hayek and Buzas, 1997); this approach has been demonstrated for a fossil plant assemblage (DiMichele et al., 1996). A regression line is fitted to the data and its slope is observed. High slopes (>1) indicate clumping, slopes on the order of one (~1) indicate a random (Poisson) distribution, and very low slopes (<1) show ordering. In the assessment of spatial distribution, quadrats are normally chosen so as to be of uniform size and to increase in size incrementally, although this is not necessarily essential (Hayek and Buzas, 1997). In the case of our surface sample data, the fallen blocks were of widely varying sizes, making the choice of uniform quadrats difficult. Selecting uniform-sized quadrats from the surfaces of the fallen blocks would have led to the exclusion of some of the already small sample.

The block sizes of the surface sample (Appendix II) are distributed according to the extreme value distribution, a highly skewed, double exponential distribution, which is the characteristic distribution of particle sizes for fractured rock (King, 1971) (Fig. 12A). Thus, there are a great many small particles (blocks) that may or may not contain stems, and very few large ones that more likely contain stems. We therefore decided to bin the block areas linearly to form three effective quadrat sizes representing 0–1 m^2, 1–2 m^2, and 2–3 m^2. The mean and variance of the number of stems in each quadrat were calculated, log-transformed, and plotted (Fig. 12B).

Using a relatively small sample, as we have, it is probable that the result would be influenced by the choice of bin size. In order to increase confidence in our result, we performed the test two more times with the data linearly divided into five and six bins representing groups of five and six effective quadrat sizes, respectively. The effective quadrat sizes thus produced were: five quadrats representing 0–0.6 m^2, 0.6–1.2 m^2, 1.2–1.8 m^2, 1.8–2.4 m^2, and 2.4–3 m^2; and six quadrats representing 0–0.5 m^2, 0.5–1 m^2, 1–1.5 m^2, 1.5-2 m^2, 2–2.5 m^2, and 2.5–3 m^2.

3.2.4. Spatial distribution – nearest neighbor

Nearest neighbor distance was estimated by three methods. (1) A randomly selected nearest neighbor distance (NND) was calculated by employing a method similar to that recommended for use with aerial photographs. We selected random points on photographs of six of the

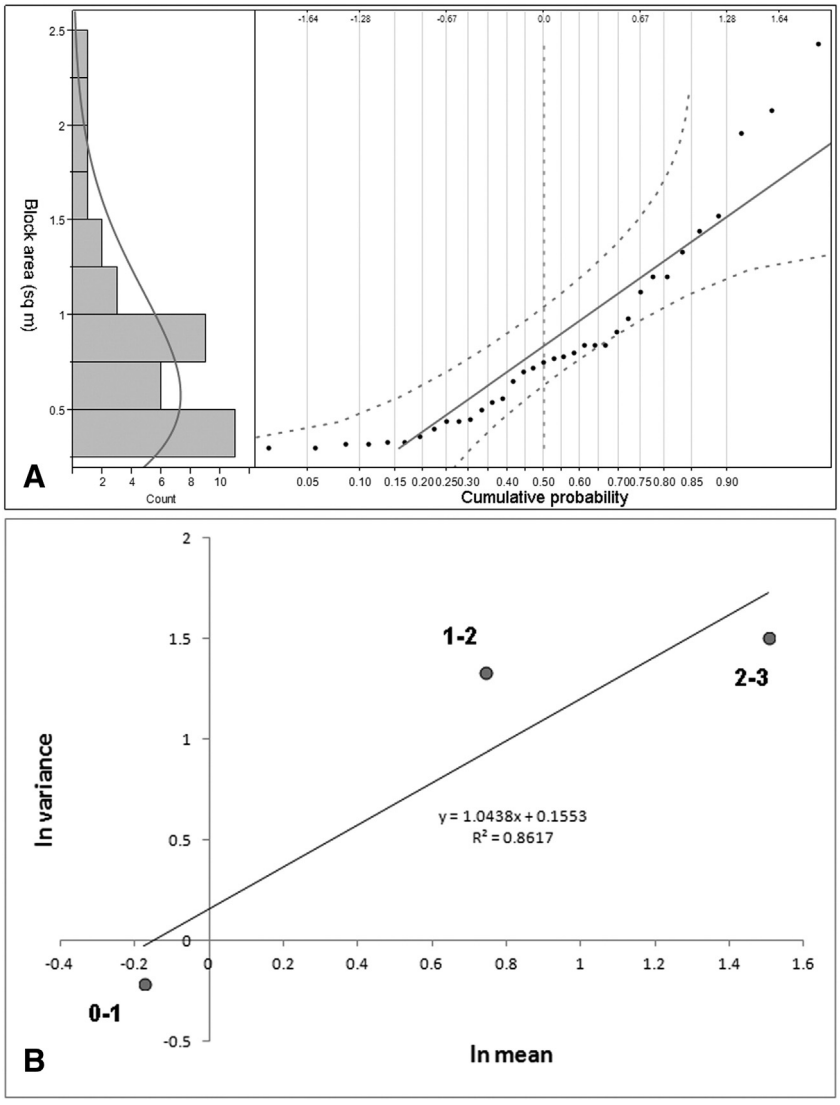

Fig. 12. Fallen block size and spacial distribution of the stems. A. Histogram and probability plot showing the highly skewed, extreme value distribution of fallen block areas. The histogram shows an extreme value curve fit. The strong concave-up shape of the data point line in the probability plot indicates high positive skew. Ordinate scale is in m^2. B. Plot of log-transformed mean versus variance for linearly binned data representing number of trees per quadrat for quadrat sizes of 0–1 m^2, 1–2 m^2, and 2–3 m^2. Slope of ~1 indicates random (Poisson) spatial distribution of the trees.

fallen block surfaces that contained stems within the central area of the block. The random points were selected by generating a pair of random numbers between zero and 100 for each block. These numbers were treated as percent of block length and percent of block width and were thus used to locate a random point on the surface of each block. The nearest plant stem to this point was the randomly selected stem, and the distance to its nearest neighbor was the random NND (Fidelibus and MacAller, 1993) (Table 1).

(2) We also calculated NND from density data. This can be done if there is a Poisson distribution of the stems in space (Dixon, 2012), which we had previously established (Fig. 12B). Thus, the mean NND is given by

$$NND_{mean} = 1/(2\rho^{1/2})$$

In which ρ equals the density.

(3) Distance to the nearest neighbor *along the transect line* ($NND_{transect}$) was measured and recorded in the field (Appendix I). This number is not to be confused with the actual nearest neighbor distance (NND_{actual}) as measured by the two methods above, because the probability is low that the actual nearest neighbor would occur on the transect line and thus be exposed for measurement; more likely, the actual nearest neighbor would be located off the transect line to either side. However, we can state that

$$NND_{actual} \leq NND_{transect}$$

because NND_{actual} cannot be greater than the observed $NND_{transect}$ along the line. Thus, we were able to approximate NND_{actual} by observing the smallest of the $NND_{transect}$ numbers.

3.2.5. Self-thinning analysis

As plant populations age, there is an accompanying increase in mean volume or mean weight of individual plants, which is further accompanied by a decrease in mean density of individuals within the stand. The density decrease is described as self-thinning and is postulated to be caused by competitively induced mortality. Once self-thinning begins, the growth of the larger, more dominant plants controls mortality in the smaller, more suppressed plants (Sackville Hamilton et al., 1995).

Self-thinning is usually displayed as a log-log plot in which the ordinate is mean volume or mean weight and the abscissa is mean density. Self-thinned plant populations tend to be distributed around a line with a −1.5 slope, which demarcates the −3/2 self-thinning rule of Yoda et al. (1963). Whereas the exact value of the slope (exponent of a power curve fit to the data) has been the subject of controversy (Norberg, 1988; Sackville Hamilton et al., 1995), all workers agree that self-thinning occurs in plant stands of sufficient maturity. White and Harper (1970) showed experimentally that the slope of the self-thinning lines in some plant population studies can vary, in their study between −1.21 and −1.7, however, these slopes generally converge on an average of −1.5.

Table 1
Randomly selected Nearest Neighbor Distances from the surface data set. Data were taken from photographs of five fallen blocks (e.g., Fig. 9A) and from the *in situ* sample (Fig. 11A).

Block number	Random % length	Random %width	Random stem diameter (cm)	NN diameter (cm)	NND (cm)
1	79	58	6.5	2	14
13	43	99	1	2	56
20	86	48	1.5	4.5	79
22	20	52	1	2	7
35	80	74	2	1.5	24
In situ	32	63	12	4	33
				Average	35.5

A weight calculation for the Sangre de Cristo stem material is difficult to make because we have no good evidence regarding its mass density, therefore, we based our self-thinning calculation on volume. We calculated stem volume using measured diameter, and height according to the formula of Niklas (1994) (Fig. 13), treating the stems as right circular cones. Additionally, to reduce the effect of the taphonomic

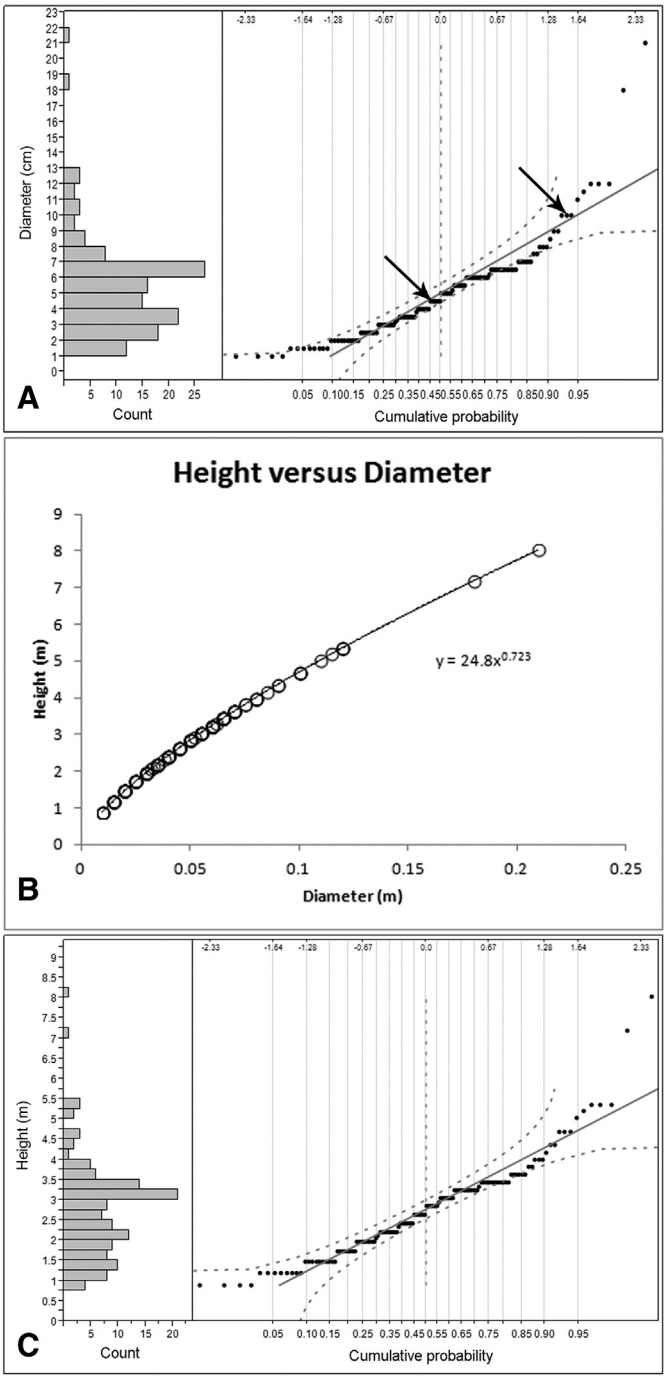

Fig. 13. Measured stem diameters and calculated heights. A. Distribution of diameters; histogram and probability plot. Multimodality is indicated by two peaks in the histogram and the two stretched-S shapes of the probability plot line. Arrows indicate inflection points of the stretched S shapes, which define the approximate boundaries of the component distributions. Positively-skewed distribution is indicated by the long positive skirt of the histogram and the concave-up probability plot data point line. Note the excursion outside the 95% Gaussian confidence intervals (dashed lines). B. Calculated height as a function of diameter over the size range of the sample. C. Distribution of heights; histogram and probability plot showing behavior similar to the diameter distribution.

reduction in the number of small stems (≤6 cm diameter), we excluded the very smallest individuals (~1 cm diameter), but we did use stems down to 2 cm in diameter to keep the sample size from becoming too small. It should be noted that the inclusion of these small diameter data (2 cm to 6 cm), which we believe to have been reduced in number by taphonomic influences, produces an artificial reduction in density and thus slightly steepens the slope of the self-thinning line. After removing the smallest individuals, 41 stems remained in the sample.

We made a first approximation of the self-thinning line by plotting linearly binned, mean volume as a function of mean density for the surface sample data.

3.3. Combined probability plots and histograms

Combined probability plots and histograms were graphed for the distribution of sizes of fallen blocks and for the distribution of stem heights and widths, measured from the transect data. The intent is for the histogram to provide a quick overview of the distribution shape, while the probability plot shows a more in-depth assessment. Interpretation of histograms is well understood by most scientists whereas probability plot interpretation may be unfamiliar to some.

Probability plotting is a simple, powerful, graphic method of comparing a data set to a statistical distribution function. Inherently, probability plots are of higher resolution than histograms because the data are not binned. A probability plot shows the probability (usually on the x axis) that a random observed variable will be less than or equal to a given value (usually on the y axis). The probability data are plotted against a scale that is related to a specific distribution function (e.g., normal, log normal, extreme value, etc.). Straight-line fits of the data on a specific probability scale therefore indicate that the data are distributed according to the function that is related to that scale. Ninety-five percent confidence intervals are provided to show if excursions in the data exceed the limits of a specific distribution type.

A probability plot more readily shows if data fit a specific distribution than a histogram. For example, in a histogram, the interpreter needs to judge how well the heights of a series of bars fit the symmetrical bell shape of a normal distribution, but in observing a probability plot the eye can readily distinguish even a small departure from a straight line. Departures from a straight line fit indicate that, for example, the data are skewed, truncated, multi-modal, or fit a different distribution function. Each of these deviations produces a unique characteristic shape on the plot that may be further explored to reveal information about the nature of the distribution and the processes or circumstances that produced it (Kock and Link, 1970; King, 1971). Additionally, important statistics such as the mean and standard deviation may be read directly off of the probability plot (mean value at the 0.5 probability level, and standard deviation at the 0.16 and 0.84 probability levels).

3.4. Geochemistry of carbonates

Seven samples of carbonate were removed for geochemical and petrographic analysis. Four of these represented the morphologies of the carbonate infilling the stem molds, including both nodular and vertically layered textures. One sample represents calcrete external to the stem mold in the adjacent sandstone. Two samples represent the calcrete nodules in the siltstone layer immediately overlying the stem-hosting sandstone. Carbonate nodules were sampled for isotopic analysis by drilling lapped slabs with an ultrafine engraving tool while viewing under a binocular microscope. The samples were analyzed for $\delta^{13}C$ and $\delta^{18}O$ by Isotech Laboratories, Inc., Champaign, Illinois. Results are reported in ppt relative to VPDB (Vienna Pee Dee Belemnite). The mineralogy of the carbonate was determined by X-ray diffraction analysis of bulk powder samples with a Bruker Phaser D2 X-ray diffractometer using Cu-kα radiation.

4. Results

4.1. Stem diameters and heights

Stem diameters varied from 2 to 21 cm, one order of magnitude. A histogram and a probability plot of the stem diameters (N = 135) show a non-normal, positively skewed distribution as indicated by the concave-up probability data-point line and by the long positive skirt of the histogram (Fig. 13A). A Shapiro-Wilk normality test confirmed that the data are not distributed normally ($W = 0.86$, $p = 6.4\times10^{-10}$); the null hypothesis of this test is that the data are normally distributed, so the low p number rejects this hypothesis.

Weak multi-modality in the data is indicated by the two long, sequential, stretched-S shapes of the probability plot data points. The long gentle flexures of the data line (as opposed to sharp jogs) show that the component distributions are thoroughly mixed (i.e., the degree of overlap of the component distributions is large). Three distinguishable component distributions (size classes) are present. The positions of the concave-up to concave-down inflection points in the data point line define the approximate "boundaries" of the three component distributions (Fig. 13A, arrows). Reading the probability between these inflections shows that about 40% of the population is in the small diameter component, about 54% is in the medium diameter component, and about 6% is in the large diameter component (Kock and Link, 1970; King, 1971; Peck, 1987).

West et al. (2009: Fig. 1) showed that the frequency distribution of plant stem sizes should decrease as the inverse square of the radius (r^{-2}) when the data are linearly binned. This results in a monotonically decreasing, concave-up curve shape for the expected diameter distribution. The early Permian stem diameter data do not show such a distribution (Fig. 13A). There are fewer stems of small diameter than expected. We hypothesize that this is due to a combination of taphonomic, geological, and observational factors.

Calculated heights varied from 0.9 m to 8.0 m, with a population mean value of ~2.6 m. A bivariate plot of height as a function of diameter based on the power equation of Niklas (1994) illustrates the relationship over the diameter range of the stems (Fig. 13B). Because the height calculations were based on diameters, the statistical distribution of heights shows the same weak multi-modality and non-normal behavior as that of the diameters (Fig. 13C). A Shapiro-Wilk normality test was performed; it also supported non-normal distribution of heights ($W = 0.927$, $\rho = 2.14\times10^{-6}$).

4.2. Stem density

Measurements made from the fallen blocks yielded a mean density estimate of 1.87 stems/m^2 or 18,700 stems/hectare. However, due to the problem of edge effects, discussed above, which may cause an underestimate of the area and a corresponding overestimate of density, we can only state with certainty that the density is ≤ 1.87 stems/m^2 in this sample. A similar measurement was made for stems visible on the top of the *in situ* sandstone bed. This sample yielded a mean density of 2.08 stems/m^2, or 20,800 stems/hectare. The average of the two density estimates is 1.98 stems/m^2. For all practical purposes, two stems/m^2 or 20,000 stems/hectare seems a good mean density estimate when all stem sizes >1 cm are included.

Density calculations based on forestry definitions of "trees" were made on the basis of the two surface samples, and thus were of small size, rendering them approximations at best. Using two minimum diameters as the bottom cut off, the >7.5 cm (N = 7) sample yielded a mean density of 0.24 stems/m^2 (2400 stems/hectare). The >10 cm (N = 4) diameter sample yielded a mean density of approximately 0.14 stems/m^2 (1400 stems/hectare).

4.3. Spatial distribution

Using the method of successively larger quadrats, a linear regression fit to the data based on three quadrat sizes shows a slope of essentially one (1.04), indicating a Poisson distribution of the trees over the sampled space (Fig. 12B). Two additional analyses with the data divided into five and six bins yielded slopes of 1.18 and 1.13, respectively; again, close enough to one to indicate a random distribution.

4.4. Nearest neighbor distance

The distribution of nearest neighbor distances in trees has been studied extensively. Normally distributed to positively-skewed nearest neighbor distances are seen in many extant wild tree populations of varying species (Hubbell, 1979; West et al., 2009, Fig. 1). The results of our three NND estimates follow:

(1) Calculated on the basis of random points on photographs of six of the fallen block surfaces (Table 1), the average NND is 35.5 cm.
(2) Nearest neighbor distance calculation based on all-stem density (Dixon, 2012) yielded 35.4 cm. If calculated on the basis of stems having >7.5 cm and >10 cm diameters, NND is approximately 1.02 m and 1.36 m, respectively.
(3) Calculated on the basis of the transect sample the average of the lowermost $NND_{transect}$ datapoints is 37.7 cm.

These three estimates, made by three different methods, are remarkably close to each other in value, thus increasing confidence in the outcome. The average of the three estimates, including stems of all sizes is 36.2 cm.

4.4.1. NND relationship to diameter

Nearest neighbor distance should increase isometrically with diameter as a result of the self-thinning, packing rule that describes how plants fill space to use available resources (Enquist et al., 2009a). In order to investigate this, we plotted all $NND_{transect}$ data as a function of diameter (Fig. 14A). The slope of the curve fit (0.9) is close to one, indicating approximate isometry. The lowermost data points were then extracted and plotted separately to approximate NND_{actual} (Fig. 14B). The slope of this line (1.3) is a bit higher than expected, but still relatively close to one. A Shapiro-Wilk test indicated a normal distribution ($W = 0.912$, $p = 0.126$) of the nearest neighbor distances.

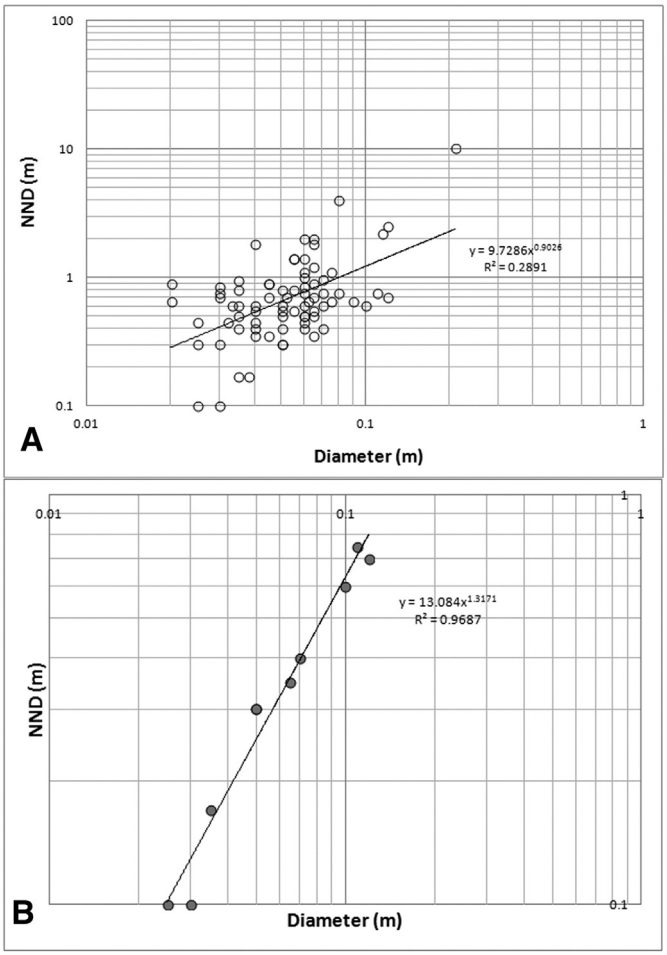

Fig. 14. Nearest neighbor distance. A. Plot of nearest neighbor distance along the transect line ($NND_{transect}$) versus diameter for all transect specimens. B. Plot of nearest neighbor distances versus diameter including only the lowermost data points from Fig. 10A. these data should approximate NND_{actual}.

4.5. Self-thinning

The slope of the self-thinning line equals the exponent of the power curve fit to the data, −1.25 in a plot of volume versus density (Fig. 16A). Because the data are binned and the sample size is small, a large influence on the curve fit is exerted by one bin (second from top) containing a single stem. The removal of this single stem from the data set improves the curve fit (note increase in R^2) and increases the slope of the self-thinning line to −1.5 (Fig. 16B).

The reasonably straight line, with its relatively gentle slope (−1.25 to −1.5), indicates that the population is self-thinning. We note that the slope of the line, with or without the questionable data point, is within the −1.21 to −1.7 range observed experimentally by White and Harper (1970) and is much lower than slopes seen in non-self-thinning populations (e.g., Norberg, 1988; Falcon-Lang, 2004).

4.6. Isotopic analysis of carbonates

The carbonate that fills the stem casts consists primarily of micritic calcite with a varying component of siliciclastic silt. XRD analyses indicate that all of the carbonate is low-Mg calcite. The isotopic analyses demonstrate consistency between the carbonate of the stem casts and the nodules in the surrounding sandstone and overlying strata. Of the four stem cast samples, mean $\delta^{13}C = 6.13‰$ (VPDB) and mean $\delta^{18}O = 5.33‰$ (VPDB). These values are nearly identical to the sample from a calcrete nodule in the adjacent sandstone host; $\delta^{13}C = 6.20‰$ (VPDB) and $\delta^{18}O = 5.23‰$ (VPDB). Additionally, the stem cast samples compare reasonably well with the two samples of calcrete from the overlying siltstone; $\delta^{13}C = 6.58, 7.07‰$ (VPDB) and $\delta^{18}O = 5.06, 4.53‰$ (VPDB).

The consistency of the results presented here demonstrates that the carbonate in the stem casts formed under the same conditions as the calcrete nodules in the surrounding sandstone. The oxygen isotope values are similar to those obtained by Tabor and Montañez (2002) from soil carbonate for western equatorial Pangaea from Virgilian through Wolfcampian-aged strata. During this time, northern New Mexico was situated in a near equatorial position (~5° N) and experienced a generally semi-arid, but seasonal climate (Tabor et al., 2008). The most noticeable difference is in the carbon isotope composition; the calcrete nodules in the siltstone layer overlying the sandstone sheet hosting the stems are slightly depleted (isotopically lighter) relative to the stem-infilling carbonate. This suggests different depths of carbonate precipitation for the two environments. Because carbonate precipitated in closer communication with the atmosphere tends to be enriched in heavier atmospheric carbon compared to the depleted

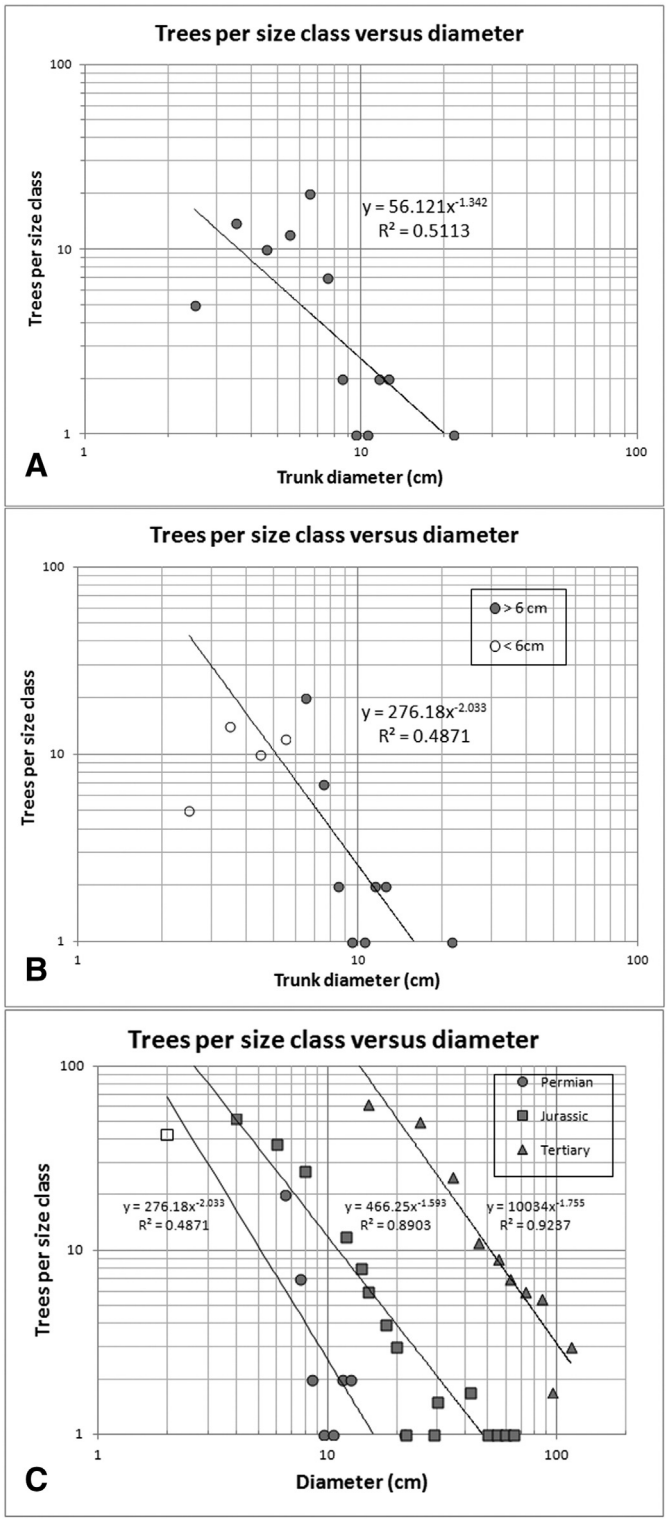

Fig. 15. Trees per size class versus diameter; log-log plot of linearly-binned data (12 bins). A. Trees per size class as a function of diameter with power curve fit to all size classes. The inverse-square relationship of number of trees to diameter dictates that the power curve exponent should equal -2, but the exponent of the power equation (slope of the line), equals -1.3. B. Similar plot with data points <6 cm diameter excluded (unfilled circles). The power equation exponent using only diameters >6 cm (filled circles) equals the predicted -2.0. C. Comparison of trees per size class as a function of diameter for three fossil woodlands: Tertiary, Jurassic, and the current early Permian sample. The unfilled square is a data point that was excluded by Enquist et al. (2007). The approximate -2 exponent is seen in all samples, but the size range increases over time in accordance with Cope's rule.

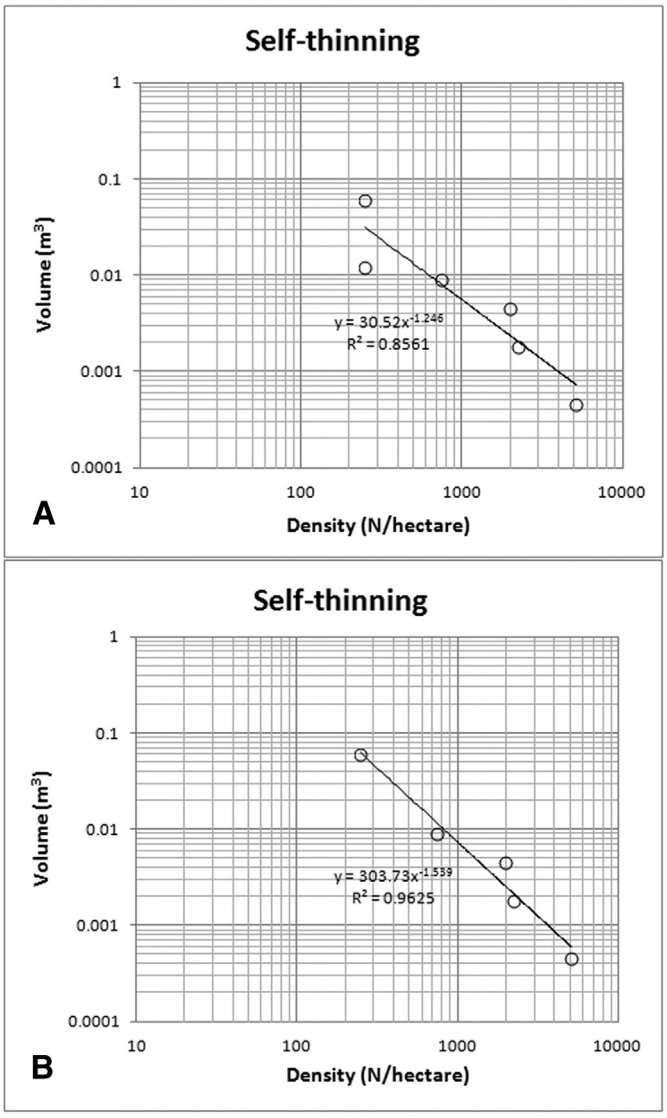

Fig. 16. Self-thinning; linearly binned data are plotted on log-log coordinates with a power curve fit. A. Bivariate plot of mean volume as a function of mean density, including all surface sample stems >1 cm diameter. Slope of the self-thinning line (exponent of the power curve) equals -1.25. B. Bivariate plot of mean volume as a function of mean density. A single data point representing one large stem has been removed thus improving the curve fit and increasing the self-thinning line slope to -1.5.

carbon respired in the deeper soil by plants (Ekart et al., 1999), the siltstone-hosted carbonate likely precipitated in a soil environment under the influence of plant respiration, while the stem-infilling carbonate experienced a stronger atmospheric effect.

Calcrete nodules in the sandstone surrounding the stems occur in only a few locations, and the sandstone itself displays very little pedogenic disturbance. Therefore, calcrete infilling of the molds is unrelated to pedogenesis of the hosting sandstone sheet. Rather, we interpret the mode of formation as involving the eventual decay of the buried stems, which extended well above the top of the sand layer at the time of death. The molds left by the decay served as conduits for both sediment and meteoric waters to the then-buried sand sheet, and allowed infill of the stem molds by precipitated carbonate.

5. Discussion

Plants preserved in situ by ash falls, floods, or mass flows have long been of significant interest to paleobotanists because of the unique information such deposits can provide on the spatial structure of ancient

vegetation. But these deposits also are of interest because they simply are evocative – plants from millions of years ago, standing as if they were buried yesterday. For the most part, such deposits represent wetland assemblages and comprise plants that are well known, often to the specific level (e.g., Libertín et al., 2009; Opluštil et al., 2009; Thomas, 2013). In situ preservation of plants from seasonally dry habitats is reported less frequently than from wetlands (Falcon-Lang et al., 2011; Bashforth et al., 2014), which is perhaps more a function of the dearth of artificial exposures, such as those created by coal mining, than an actual taphonomic bias. The deposit described here most likely never would have been discovered were it not for commercial quarrying of the host rock for flagstone. Yet, where such seasonally dry assemblages are reported, identification of the plants can present significant challenges.

The identity of the plants preserved within the early Permian flood-deposited sandstone described herein is uncertain because of the lack of preservation of definitive characteristics. Our best inference is that these plants are some kind of coniferophyte, perhaps *Dicranophyllum*, though it is possible they are of unknown affinity. The large population of stem molds, >150 individuals, has no gross morphological features that would permit assignment to the calamitaleans, arborescent lycopsids, or marattialean tree ferns. The centralized rooting, relatively thin stems, and possible induction of adventitious rooting and lateral shoots by burial in sediment are consistent with either a pteridosperm or coniferopsid affinity. And, the rare presence of long, linear leaves points to a possible dicranophyll identity. The *Walchia piniformis* branches found in loose blocks within the quarries, but from uncertain beds, are unlikely candidates for association, given what is known of the walchian conifer growth habit (Hernandez-Castillo et al., 2003; Looy, 2013).

Whatever these stems may represent taxonomically, the vegetation they form is unlike any other reported from the Paleozoic – a dense stand, perhaps as many as 20,000 individuals per hectare, of moderate sized, to small stems, ranging from 2 to 21 cm in diameter. It is difficult to call such plants trees, given their modest dimensions. The plants are centrally rooted and appear not to have been clonal. The calamitaleans are the only other group documented to have the capacity to recover from burial such as that described here (e.g., Gastaldo, 1992; Pfefferkorn et al., 2001), but these stems lack any of the highly distinctive, stereotypical architectural features of that group.

The plants in question appear to have been colonizers of seasonally dry floodplain soils, though the length or intensity of the seasonal moisture deficit cannot be determined from the thin, immature, sandy soils in which the rooting bases are preserved. The stems in the smaller northwest quarry exposure include some that appear to have colonized a scour surface through an underlying sandstone bed that had buried an earlier plant stand. Furthermore, there is no unequivocal evidence that the stems represent more than a single species, based on the preserved morphological characteristics. From these various lines of evidence, we infer that the plants were living in environments subject to periodic, flashy floods of relatively high intensity, perhaps on cycles of decades to 100 years. In at least those locations where the stems are preserved, the floods were sufficiently widely spaced in time to permit the development of multiple generations of plants on the landscape. Climatic indicators, such as pedogenic carbonate in soils within the local stratigraphic section, also suggest periodicity of rainfall. The temporally equivalent Abo Formation has been interpreted to have formed under a strongly seasonal, semi-arid to sub-humid climate regime (Mack et al., 1991, 2010; Mack, 2003; Tabor et al., 2008), which, in combination with the disturbance regime, may have limited species diversity. As occupants of what appear to be areas of potentially frequent, large scale floods, the plants in question may have preferentially grown in environments with greater or more reliable moisture availability than better drained or slightly higher elevation interfluve regions between channel belts, which were probably dominated by walchian conifers, given the composition of the flora from the coeval Abo Formation (DiMichele et al., 2013).

5.1. Stem diameters and height

The distribution of tree diameters in extant forests has been well studied. Positively skewed distribution of diameters in extant, wild tree populations is predicted, and has been observed (Mohler et al., 1978; Enquist et al., 2007; West et al., 2009). A histogram and probability plot of the early Permian tree diameters (N = 135) also show a non-normal, positively-skewed distribution as indicated by the overall concave-up probability data point line and by the long positive skirt of the histogram (Fig. 13A).

The indication of stem-size multi-modality, though weak, may indicate the presence of age-based size classes, mixed species, or sexual dimorphism. Multi-modality in size distributions is characteristic of biological data when such underlying factors are at play. The likelihood of mixed species seems remote, based on the morphological similarity of the stems, regardless of diameter – that is, the presence of what appear to be adventitious branches and roots, the elongate stems, and the bell-shaped rooting bases. But if the three size classes represent > 1 species, the size distributions of these species, in terms of stem diameter, overlap greatly.

Many of the individual scaling relationships of plants such as lengths (heights), body masses, and growth rates show constant, simple allometry, thus enabling the reliable calculation of these parameters (Niklas and Enquist, 2001). These allometric relationships persist over sizes that range from single-celled organisms to the largest trees (~ six orders of magnitude in length). We used such an allometric relation to calculate stem heights based on the power equation of Niklas (1994).

5.2. Potential taphonomic biases in the detection of small plants

The Sangre de Cristo Formation assemblage was buried in sand to a depth of approximately one meter by fluvial processes. Thus, there is some probability that smaller plants were present but were preferentially knocked flat and thus were not preserved in upright position, particularly in light of a flood sufficient to deposit a meter of sand. This possibility is suggested by the observation that many of the smaller stems are inclined to the south, whereas all of the larger stems are nearly vertical (Figs. 3A, 5A-C). There is an additional possibility that the smaller stems would not concentrate stress sufficiently in the rock to cause a joint to propagate through them and thus facilitate their exposure. Additionally, smaller stems might not be detected by the observers, even if preserved and exposed. Indeed, during data collection at NMMNH locality 9082, it was noted that the smaller stems contained little or no carbonate infilling and were much more difficult to locate on outcrop.

Other factors, in addition to those mentioned above, may affect the probability of preservation. We thus conclude that the smaller the diameter of the stem, the greater the likelihood that it has not been recorded in the database and that the shape of the diameter distribution, particularly in the smaller size classes, is greatly affected by extrinsic taphonomic factors that lie outside the dynamics of the plant population itself. Only trees of greater than 6 cm diameter seem to follow the expected concave-up distribution shape (Fig. 13A, histogram).

5.3. Size-frequency distribution

As a result of the inverse square rule of size-frequency distribution, an allometric constant of −2 should be found between the number of trees/size class and the trunk diameter in linearly binned data (Enquist et al., 2009a). After linear binning of the stem diameters

(12 bins), we show an allometry plot of stems per size class as a function of diameter (Fig. 15A). The allometric constant (slope) of −1.3 is well below the value found for modern vegetation. However, when we exclude stems of ≤6 cm diameter, a size class we have concluded to be significantly influenced by taphonomic factors, the slope increases to the expected −2.0 (Fig. 15B). This result seems to support the idea that a good representative sample of the larger stems is preserved and that many of the stems originally part of the stand but ≤ 6 cm in diameter are missing due to preservational biases or were undetected. Although there are many reports of in situ vegetation from the fossil record, few have been analyzed, or the data reported, in a manner that would permit an analysis of the size-frequency distribution. There are a small number of such examples, however.

Enquist et al. (2007, Fig. 8) compared the diameter distributions of Jurassic and early Tertiary fossil forests. Their plot of number of stems per size class as a function of diameter showed similar slopes for the two forests. The Jurassic forest was dominated by gymnosperms (conifers) with a well developed undergrowth of osmundaceous ferns (Pole, 1999). The early Tertiary forest comprised mostly gymnosperms and angiosperms (Basinger et al., 1994), including some extant genera. Both the Jurassic and the early Tertiary data are from polar or near-polar forests, as opposed to our near-equatorial early Permian assemblage. However, Pole (1999) states that there are no structural aspects of the near-polar Jurassic forest to distinguish it from medium or low latitude forests. Both of these younger assemblages were composed of multiple species, whereas the Permian assemblage is most likely monospecific or of very low diversity.

We extracted the Jurassic and early Tertiary diameter data from Enquist et al. (2007, Fig. 8) and added our early Permian data in a comparative plot of trees per size class versus diameter for the three time periods (Fig. 15C). The Permian data are for those stems with diameters >6 cm diameter. The slopes of all three data point lines are relatively close to −2 and are all well within the range of similar data for extant forests (Enquist et al., 2007, Fig. 6).

5.4. Self-thinning

As noted, the early Permian woodland described here demonstrates self-thinning effects. Self-thinning is seen in essentially all terra firma plant populations, regardless of plant size – from mosses and grasses to the largest trees. Plants reach their self-thinning limit at an age that is based on the available resources of the site. Studies show that a few decades (30–45 years) may be required for tree stands to attain self-thinning densities (Gibson and Good, 1986), whereas grasses may do so in a matter of weeks (White and Harper, 1970).

In plant stands that have not yet reached self-thinning, the slope of the data line in a self-thinning plot is very steep. This line curves upward to the left and its slope grows gentler as the plants approach self-thinning. This effect was explored and discussed theoretically by Norberg (1988) and was observed by Falcon-Lang (2004) in Early Mississippian-aged lycopsid forests.

Sackville Hamilton et al. (1995) argued convincingly that it is competition for light rather than nutrients that drives self-thinning because increasing light intensity shifts the self-thinning line upward (toward greater volume or weight), whereas increasing nutrients only increases the rate of a population's progression up the line without changing its position. This observation fits well with the idea that canopy radius may limit Nearest Neighbor Distance (NND).

6. Summary

Flood-deposited layers of fine, crossbedded sandstone in the early Permian (Wolfcampian) Sangre de Cristo Formation of northern New Mexico contain a large number of natural molds of plant stems. The statistical sample size (N > 165), and the area over which one of these deposits occurs, is sufficient to allow a rare assessment of the dynamics of the woodland that it represents. The taxonomy of the stems is difficult to access, but the available evidence suggests they may be coniferophytic gymnosperms, possibly dicranophylls. A monospecific assemblage seems likely from the morphological evidence, but distinct size classes in the data raise the possibility of mixed species. The stem diameters comprise three overlapping size classes that contain, in order of increasing size, ~40%, ~54%, and ~6% of the population. We suspect that the smallest size class is artificially reduced by outside influences (explained below).

The stems vary in diameter from 1 cm up to 21 cm with corresponding calculated heights of ~0.9 m up to >8 m. A few of the stems reach the modern forestry definitions of “tree size,” being greater than 7.5 cm (7 stems) or 10 cm (4 stems) in diameter. The anticipated stem diameter size distribution in which the number of stems decreases with a −2 exponent (inverse square law) is present in the sample, but only in stems >6 cm. Observations on the outcrop, where many of the stems ≤6 cm diameter are seen to be bent over suggest a taphonomic explanation: that the initial inundation selectively flattened the smallest members of the population and removed them from the sample.

Density calculations for the stand showed approximately 20,000 stems per hectare including all size classes. The density of the tree-sized stems of >7.5 cm or >10 cm diameter was an order of magnitude lower, 2400 and 1400 stems/hectare respectively.

The plant stems are distributed randomly over the area of the stand. We have shown that their spatial distribution fits a Poisson probability distribution function, which probably indicates healthy competition between the plants. Nearest neighbor distance for the entire stand was ~36 cm with the >7.5 cm and >10 cm diameter stems showing ~1 m and ~1.4 m NNDs respectively. NND increased in isometry with respect to diameter indicating that the early Permian stems were following the same packing rule as extant plant stands in their use of available space and resources.

In a size-frequency comparison of stems per size class versus diameter, the early Permian stand showed behavior very similar to that of Jurassic and Tertiary fossil tree stands, and were found to be well within the range of extant woodlands. Cope's rule (Cope, 1887) apparently applies to the plant data because the stems per size class-to-diameter ratio holds approximately constant over time, but size increases.

The early Permian woodland was shown to be self-thinning. Its self-thinning exponent is between −1.25 and −1.5, probably very close to −1.5. These values are within the range seen in the experiments of White and Harper (1970) using extant plant stands.

Acknowledgments

We thank the U.S. Bureau of Land Management, particularly Regional Paleontologist Philip Gensler, for cooperation in granting access to the area in which this research was carried out. Comments from two anonymous reviewers, which led to improvements in the paper, are sincerely acknowledged.

Appendix I

Transect sample; trees exposed in growth position along N-S-trending highwall of lower BLM quarry SW of San Miguel, NM, measured 5-31-13. Numbers were assigned from north to south along the transect line. Missing data in the diameter column reflect specimens in which poor preservation or exposure precluded

reliable measurement. Distance to nearest neighbor indicates nearest neighbor along the transect line, not necessarily the actual nearest neighbor, which may not be located on the line.

Number	Distance to next tree (m)	Distance to nearest neighbor (m)	Diameter (m)
1		0.3	0.03
2	0.3	0.3	
3	5.3	0.3	0.025
4	10.1	2	0.065
5	2	10.1	0.21
6	13.9	2	0.06
7	9.2	4	0.08
8	4	0.6	0.033
9	0.6	0.17	0.038
10	0.17	0.1	0.03
11	0.1	0.17	0.035
12	2.2	0.1	0.025
13	2.3	2.2	0.115
14	2.5	1.81	0.04
15	1.81	1.1	
16	1.1	1.81	0.065
17	2.1	1.1	0.075
18	1.8	1.4	0.055
19	1.4	0.55	0.05
20	0.55	1.4	0.06
21	1.8	0.55	0.04
22	1.2	0.97	
23	0.97	1.2	
24	2.95	0.97	0.07
25	1.1	0.8	0.055
26	0.8	1.1	0.06
27	2.4	0.7	
28	0.7	0.45	0.032
29	0.45	0.7	0.052
30	0.85	0.45	0.025
31	0.85	0.9	0.045
32	0.9	0.85	0.03
33	1.5	0.9	
34	1.1	1.4	0.055
35	1.4	0.65	0.09
36	0.65	0.95	0.035
37	0.95	0.65	
38	0.65	0.75	0.08
39	0.75	0.65	0.075
40	0.8	0.75	0.07
41	0.75	0.5	0.06
42	0.5	0.7	
43	0.7	0.5	0.035
44	0.7	0.7	0.045
45	1.2	0.6	0.04
46	0.6	0.8	0.035
47	0.8	0.6	0.06
48	0.6	0.65	
49	0.65	0.6	0.035
50	1.2	0.65	0.062
51	1	1.2	0.065
52	1.7	0.5	
53	0.5	0.55	0.055
54	0.55	0.5	0.06
55	0.5	0.55	
56	3.8	0.5	
57	1.2	0.35	0.04
58	0.35	0.7	0.065
59	0.7	0.35	0.065
60	0.95	0.7	
61	1.5	0.5	
62	0.5	0.75	
63	0.75	0.4	0.035
64	0.4	0.75	0.03
65	1.45	0.4	0.04
66	0.5	0.75	0.06
67	0.75	0.5	
68	0.8	0.6	
69	0.6	0.8	0.05
70	0.9	0.45	0.06
71	0.45	0.4	0.05
72	0.4	0.45	
73	1	0.4	0.07
74	1.4	0.9	0.02
75	0.9	1.1	
76	1.1	0.4	0.06
77	0.4	1	
78	1	0.2	
79	0.2	0.7	0.03
80	0.7	0.2	
81	14	0.7	0.12
82	1.6	1	0.06
83	1	0.9	
84	0.9	0.65	0.02
85	0.65	0.9	0.065
86	0.9	0.65	
87	0.65	0.3	0.05
88	0.3	0.6	
89	0.6	0.3	0.05
90	0.55	0.6	0.05
91	1	0.55	0.065
92	0.6	0.75	
93	0.75	0.6	
94	0.9	0.5	0.05
95	0.5	0.75	0.11
96	0.75	0.5	0.065
97	0.85	0.45	0.04
98	0.45	0.85	
99	0.9	0.45	
100	1.7	0.9	0.045
101	1.2	0.6	
102	0.6	0.6	
103	0.6	0.6	0.1
104	0.7	0.6	0.07
105	1	0.7	
106	2	0.35	
107	0.35	0.85	
108	0.85	0.35	0.045
109	2.5	0.85	0.06
110	3.4	2.5	0.12

Appendix I (*continued*)

Appendix II

Surface sample; approximate length, width, surface area, and number of trees contained within each of 35 fallen blocks of the tree-bearing sandstone.

Block number	Length (m)	Width (m)	Area m^2	Number trees in block
1	1.3	0.7	0.91	10
2	1.3	0.6	0.78	1
3	1.2	0.45	0.54	2
4	1.1	0.3	0.33	2
5	1.2	0.7	0.84	0
6	1.1	0.4	0.44	1
7	1.1	0.4	0.44	0
8	1.6	0.5	0.8	1
9	1	0.3	0.3	0
10	1.1	0.3	0.33	1
11	0.7	0.8	0.56	0
12	0.9	0.5	0.45	1
13	2.7	0.9	2.43	3
14	1	0.3	0.3	0
15	0.8	0.4	0.32	1
16	0.9	0.4	0.36	0
17	0.7	1.2	0.84	0
18	1.2	0.6	0.72	2
19	0.8	0.5	0.4	0
20	2.6	0.8	2.08	6
21	2	0.6	1.2	1
22	1.5	0.8	1.2	2
23	1.4	1.4	1.96	1

Appendix II (*continued*)

Block number	Length (m)	Width (m)	Area m^2	Number trees in block
24	1.3	0.5	0.65	1
25	1.2	0.7	0.84	0
26	1.4	0.7	0.98	1
27	1	0.5	0.5	0
28	1.4	0.8	1.12	0
29	1	0.7	0.7	0
30	1.9	0.8	1.52	2
31	0.7	1.1	0.77	2
32	0.8	0.4	0.32	3
33	0.9	1.6	1.44	3
34	0.5	1.5	0.75	2
35	1.9	0.7	1.33	6
		Sums	29.45	55

Appendix III

Surface sample; diameters of trees contained within fallen blocks of the tree-bearing sandstone. Diameters were measured well above the basal flair of the tree stems. The original upright orientation of the blocks was determined by crossbedding set relationships. Those designated "*in situ*" were exposed in cross section in the quarry highwall by removal of overburden from the tree-bearing layer.

Block number	Diameters (m)
1	0.1
	0.02
	0.015
	0.015
	0.065
	0.025
	0.02
	0.065
	0.025
	0.03
2	0.08
3	0.085
	0.065
4	0.025
	0.03
6	0.07
8	0.015
10	0.02
12	0.045
13	0.025
	0.01
	0.02
15	0.18
18	0.035
	0.015
20	0.045
	0.01
	0.015
	0.015
	0.015
	0.01
21	0.02
22	0.02
	0.01
23	0.04
24	0.1
26	0.065
30	0.03
	0.03
31	0.035
	0.025
32	0.055
	0.065
	0.055

Appendix III (*continued*)

Block number	Diameters (m)
33	0.055
	0.02
	0.07
34	0.055
	0.035
35	0.035
	0.06
	0.04
	0.015
	0.02
	0.045
in situ	0.12
	0.09
	0.06

References

Anderson, D.R., Laake, J.L., Crain, B.R., Burnham, K.P., 1979. Guidelines for line transect sampling of biological populations. J. Wildl. Manag. 43, 70–78.

Baltz, E.H., Myers, D.A., 1999. Stratigraphic framework of upper Paleozoic rocks, southeastern Sangre de Cristo Mountains, New Mexico, with a section on speculations and implications for regional interpretation of Ancestral Rocky mountains paleotectonics. New Mex. Bur. Min. Mineral Resour. Mem. 48 (269 p. and 5 plates).

Barthel, M., Noll, R., 1999. On the growth habit of *Dicranophyllum hallei* Remy et Remy. Veröffentlichungen des Naturhistorischen Museums Schleusingen 14 pp. 59–64.

Barthel, M., Bettag, E., Noll, R., 1998. *Dicranaophyllum hallei* Remy et Remy im oberen Rotliegend. Veröffentlichungen des Museum für Naturkunde Chemnitz 21 pp. 5–20.

Bashforth, A.R., Cleal, C.J., Gibling, M.R., Falcon-Lang, H.J., Miller, R.F., 2014. Paleoecology of Early Pennsylvanian vegetation on a seasonally dry tropical landscape (Tynemouth Creek Formation, New Brunswick, Canada). Rev. Palaeobot. Palynol. 200, 229–263.

Basinger, J.F., Greenwood, D.R., Sweda, T., 1994. Early tertiary vegetation of arctic Canada and its relevance to paleoclimatic interpretation. In: Boulter, M.C., Fisher, H.C. (Eds.), Cenozoic plants and climates of the arctic. Springer, Berlin, pp. 175–198.

Berman, D.S., Henrici, A.C., Lucas, S.G., 2013. *Ophiacodon* (Synapsida, Ophiacodontidae) from the Lower Permian Sangre de Cristo Formation of New Mexico. N. M. Mus. Nat. Hist. Sci. Bull. 60, 36–41.

Buck, S.G., Goldring, R., 2003. Conical sedimentary structures, trace fossils or not? Observations, experiments, and review. J. Sediment. Res. 73, 338–353.

Burnham, K.P., Anderson, D.R., Laake, 1980. Estimation of density from line transect sampling of biological populations. Wildlife Monographs No. 72John Wiley & Sons, New York (on behalf of the Wildlife Society, 3–202).

Chamberlain, C.J., 1966. Gymnosperms: structure and evolution. Dover Publications Incorporated, New York (484 pp.).

Cope, E.D., 1887. The origin of the fittest: essays on evolution. Appleton, New York (467 pp.).

DiMichele, W.A., Falcon-Lang, H.J., 2011. Pennsylvanian 'fossil forests' in growth position (T^0 assemblages): origin, taphonomic bias and palaeoecological insights. J. Geol. Soc. 168, 585–605.

DiMichele, W.A., Phillips, T.L., 1996. Clades, ecological amplitudes and ecomorphs: Phylogenetic effects and persistence of primitive plant communities in the Pennsylvanian-age tropical wetlands. Palaeogeogr. Palaeoclimatol. Palaeoecol. 127, 83–105.

DiMichele, W.A., Elbe, C.F., Chaney, D.S., 1996. A drowned lycopsid forest above the Mahoning coal (Conemaugh Group, Upper Pennsylvanian) in eastern Ohio, U.S.A. Int. J. Coal Geol. 31, 249–276.

DiMichele, W.A., Chaney, D.S., Lucas, S.G., Kerp, H., Voigt, S., 2013. Flora of the Lower Permian Abo Formation redbeds, western equatorial Pangea, New Mexico. N. M. Mus. Nat. Hist. Sci. Bull. 59, 265–287.

Dixon, P.M., 2012. Nearest neighbor methods. In: El-Shaarawi, A.-H., Piegorsch, W. (Eds.), Encyclopedia of environmetrics, 2nd ed. John Wiley & Sons Ltd, Chichester, UK, pp. 1743–1756 http://dx.doi.org/10.1002/9780470057339.van007.pub2.

Ekart, D.D., Cerling, T.E., Montanez, I.P., Tabor, N.J., 1999. A 400 million year carbon isotope record of pedogenic carbonate: implications for paleoatmospheric carbon dioxide. Am. J. Sci. 299, 805–827.

Enquist, B.J., Tiffney, B.H., Niklas, K.J., 2007. Metabolic scaling and the evolutionary dynamics of plant size, form, diversity: toward a synthesis of ecology, evolution, paleontology. Int. J. Plant Sci. 168, 729–749.

Enquist, B.J., West, G.B., Brown, J.H., 2009a. Extensions and evaluations of a general quantitative theory of forest structure and dynamics. Proc. Natl. Acad. Sci. 106, 7046–7051.

Falcon-Lang, H.J., 2004. Early Mississippian lycopsid forests in a delta-plain setting at Norton, near Sussex, New Brunswick, Canada. J. Geol. Soc. 161, 969–981.

Falcon-Lang, H.J., Jud, N.A., Nelson, W.J., DiMichele, W.A., Chaney, D.S., Lucas, S.G., 2011. Pennsylvanian coniferopsid forests in sabkha facies reveal the nature of seasonal tropical biome. Geology 39, 371–374.

Falcon-Lang, H.J., Lucas, S.G., Kerp, H., Krainer, K., Montañez, I.P., Vachard, D., Chaney, D.S., Elrick, S.D., Contreras, D.L., Kurzawe, F., DiMichele, W.A., Looy, C.V., 2015. Early Permian (Asselian) vegetation from a seasonally dry coast in western equatorial Pangaea: Paleoecology and evolutionary significance. Palaeogeogr. Palaeoclimatol. Palaeoecol (submitted for publication).

Fidelibus, M.W., MacAller, R.T.F., 1993. Methods for plant sampling, Restoration in the Colorado Desert: Management Notes, Prepared for California Department of Transportation, San Diego. pp. 1–7.
Gastaldo, R.A., 1992. Regenerative growth in fossil horsetails following burial by alluvium. Hist. Biol. 6, 203–219.
Gibson, D.J., Good, R.E., 1986. Population structure and thinning in natural stands of Atlantic white cedar (*Chamaecyparis thyoides* (L.) BSP). Oecologia 69, 348–353.
Gregorie, T.G., Valentine, H.T., 2003. Line intersect sampling: Ell-shaped transects and multiple intersections. Environ. Ecol. Stat. 10, 263–279.
Hammer, Ø., Harper, D.A.T., Ryan, P.D., 2001. PAST Paleontological Statistics Software Package for education and data analysis. Palaeontol. Electron. 4 (9 pp., http://palaeo-electronica.org/2001_1/past/issue1_01.htm).
Hayek, L.-A.C., Buzas, M.A., 1997. Surveying natural populations. Columbia University Press, New York (563 pp.).
Hernandez-Castillo, G.R., Rothwell, G.W., Stockey, R.A., Mapes, G., 2003. Growth architecture of *Thucydia mahoningensis*, a model for primitive walchian conifer plants. Int. J. Plant Sci. 164, 443–452.
Hernandez-Castillo, G.R., Stockey, R.A., Rothwell, G.W., Mapes, G., 2009. Reconstructing *Emporia lockardii* (Voltziales: Emporiaceae) and initial thoughts on Paleozoic conifer ecology. Int. J. Plant Sci. 170, 1056–1074.
Hubbell, S.P., 1979. Tree dispersion, abundance, and diversity in a tropical dry forest. Science 203, 1299–1309.
Hunt, A.P., Lucas, S.G., Huber, P., 1990. Early Permian footprints from the Sangre de Cristo Formation of northeastern New Mexico. N. M. Geol. Soc. Field Conf. Guideb. 41, 291–303.
Jefferson, T.H., 1982. Fossil forests from the Lower Cretaceous of Alexander Island, Antarctica. Palaeontology 25, 681–708.
JMP 10.0.0, 2012. Statistical analysis software. SAS Institute Incorporated, SAS Campus Drive, Building T, Cary, NC 27513.
Kerp, H., Noll, R., Uhl, D., 2007. Vegetationsbilder aus dem saarpfälzischen Permokarbon. In: Schindler, T., Heidtke, U.H.J. (Eds.), Kohlesümpfe, Seen und Halbwüsten. Pollichia Sonderveröffentlichung 10, pp. 76–109.
King, J.R., 1971. Probability charts for decision making. Industrial Press Incorporated, New York (290 pp.).
Kock Jr., G.S., Link, R.F., 1970. Statistical analysis of geological data. Dover Publications, Inc., New York (438 pp.).
Krainer, K., Lucas, S.G., 1995. The limestone facies of the Abo–Hueco transitional zone in the Robledo Mountains, southern New Mexico. N. M. Mus. Nat. Hist. Sci. Bull. 6, 33–38.
Legendre, P., Fortin, M.J., 1989. Spatial pattern and ecological analysis. Vegetatio 80, 107–138.
Libertín, M., Opluštil, S., Pšenička, J., Bek, J., Sýkorov, I., Dašková, J., 2009. Middle Pennsylvanian pioneer plant assemblage buried *in situ* by volcanic ash-fall, central Bohemia, Czech Republic. Rev. Palaeobot. Palynol. 155, 204–233.
Long, J.C.S., Aydin, A., Brown, S.R., Einstein, H.H., Hestir, K., Hsieh, P.A., Meyer, L.R., Nolte, K.G., Norton, D.L., Olsson, O.L., Paillet, F.L., Smith, J.L., Thomsen, L., 1996. Rock fractures and fluid flow: Contemporary understanding and applications. National Academy Press, Washington D.C. (551 pp.).
Looy, C.V., 2007. Extending the range of derived Late Paleozoic conifers: *Lebowskia* gen. nov. (Majonicaceae). Int. J. Plant Sci. 168, 957–972.
Looy, C.V., 2013. Natural history of a plant trait: branch-system abscission in Paleozoic conifers and its environmental, autecological, and ecosystem implications in a fire-prone world. Paleobiology 39, 235–252.
Lucas, S.G., 2005. Permian tetrapod faunachrons. N. M. Mus. Nat. Hist. Sci. Bull. 30, 197–201.
Lucas, S.G., 2006. Global Permian tetrapod biostratigraphy and biochronology. In: Lucas, S.G., Schneider, J.W., Cassinis, G. (Eds.), Nonmarine Permian chronology and correlation. Geological Society Special Publication 265, pp. 65–93.
Lucas, S.G., Heckert, A.B., Estep, J.W., Hunt, A.P., Anderson, O.J., 1998. Stratigraphy, paleontology and depositional environments of the Lower Permian Robledo Mountains Formation of the Hueco Group, Robledo Mountains, New Mexico. N. M. Mus. Nat. Hist. Sci. Bull. 12, 29–41.
Lucas, S.G., Krainer, K., Colpitts Jr., R.M., 2005. Abo-Yeso (Lower Permian) stratigraphy in central New Mexico. N. M. Mus. Nat. Hist. Sci. Bull. 31, 101–117.
Lucas, S.G., Krainer, K., Chaney, D.S., DiMichele, W.A., Voigt, S., Berman, D.S., Henrici, A.C., 2012a. The Lower Pemian Abo Formation in the Fra Cristobal and Caballo Mountains, Sierra County, New Mexico. N. M. Geol. Soc. Guideb. 63, 345–376.
Lucas, S.G., Harris, S.K., Spielmann, J.A., Berman, D.S., Henrici, A.C., Krainer, K., Rinehart, L.F., DiMichele, W.A., Chaney, D.S., Kerp, H., 2012b. Lithostratigraphy, paleontology, biostratigraphy and age of the upper Paleozoic Abo Formation near Jemez Springs, northern New Mexico, USA. Ann. Carnegie Mus. 80, 323–350.
Lucas, S.G., Krainer, K., Chaney, D.S., DiMichele, W.A., Voigt, S., Berman, D.S., Henrici, A.C., 2013. The Lower Permian Abo Formation in central New Mexico. N. M. Mus. Nat. Hist. Sci. Bull. 59, 161–180.
Mack, G.H., 2003. Lower Permian terrestrial paleoclimatic indicators in New Mexico and their comparison to paleoclimate models. N. M. Geol. Soc. Guideb. 54, 231–234.
Mack, G.H., Cole, D.R., Giordano, T.H., Schaal, W.C., Barcelos, J.D., 1991. Paleoclimatic controls on stable oxygen and carbon isotopes in caliche of the Abo Formation (Permian), south-central New Mexico, USA. J. Sediment. Petrol. 61, 458–472.
Mack, G.H., Tabor, N.J., Zollinger, H.J., 2010. Palaeosols and sequence stratigraphy of the Lower Permian Abo Member, south-central New Mexico, USA. Sedimentology 57, 1566–1583.
Mamay, S.G., 1967. Lower Permian plants from the Arroyo Formation in Baylor County, north-central Texas. U. S. Geol. Surv. Prof. Pap. 575-C, 120–126.
Mohler, C.L., Marks, P.L., Sprugel, D.G., 1978. Stand structure and allometry of trees during self-thinning of pure stands. J. Ecol. 66, 599–614.
Mosbrugger, V., Gee, C.T., Belz, G., Ashraf, A.R., 1994. Three-dimensional reconstruction of an in situ Miocene peat forest from the Lower Rhine Embayment, northwestern Germany – new methods in paleovegetation analysis. Palaeogeogr. Palaeoclimatol. Palaeoecol. 110, 295–317.
Nelson, W.J., Elrick, S.D., Lucas, S.G., 2013. Clastic dike in the late Paleozoic Bursum Formation at Carrizo Arroyo, New Mexico – A likely paleoseismic sand blow. N. M. Mus. Nat. Hist. Sci. Bull. 59, 31–33.
Niklas, K.J., 1994. The allometry of safety-factors for plant height. Am. J. Bot. 81, 345–351.
Niklas, K.J., Enquist, B.J., 2001. Invariant scaling relationships for interspecific plant biomass production rates and body size. Proc. Natl. Acad. Sci. 98, 2922–2927. http://dx.doi.org/10.1073/pnas.041490298.
Norberg, R.Å., 1988. Theory of growth geometry of plants and self-thinning of plant populations: Geometric similarity, Elastic similarity, and different growth modes of plant parts. Am. Nat. 131, 220–256.
Odier, G., Hasiotis, S.T., Rasmussen, D., McCormick, T., 2006. Preliminary report on dewatering pipes in the lower part of the Lower Jurassic Navajo Sandstone, Canyonlands National Park, southeastern Utah; implications for pluvial episodes and the occurrence of lakes, trees, mammal burrows. Abstr. Programs Geol. Soc. Am. 38 (7), 144–145.
Opluštil, S., Pšenička, J., Libertín, M., Bashforth, A.R., Šimůnek, Z., Drábková, J., Dašková, J., 2009. A Middle Pennsylvanian (Bolsovian) peat-forming forest preserved in situ in volcanic ash of the Whetstone Horizon in the Radnice Basin, Czech Republic. Rev. Palaeobot. Palynol. 155, 234–274.
Peck, D.S., 1987. Accelerated testing handbook. Technology Associates, Portola, CA (136 pp.).
Pfefferkorn, H.W., Wang, J., 2007. Early Permian coal-forming floras preserved as compressions from the Wuda District (Inner Mongolia, China). Int. J. Coal Geol. 69, 90–102.
Pfefferkorn, H.W., Archer, A.W., Zodrow, E.L., 2001. Modern tropical analogs for Carboniferous standing forests: Comparison of extinct *Mesocalamites* with extant *Montrichardia*. Hist. Biol. 15, 235–250.
Pole, M., 1999. Structure of a near-polar latitude forest from the New Zealand Jurassic. Palaeogeogr. Palaeoclimatol. Palaeoecol. 147, 121–139.
Renault, B., Zeiller, R., 1888. Ètudes sur le terrain houllier de Commentry, Livre 2, Flore fossile, Pt I. Bulletin de la Société de l'Industrie Minerale St.-Etienne 2 pp. 1–366.
Sackville Hamilton, N.R., Matthew, C., Lemaire, G., 1995. In defense of the −3/2 boundary rule: a re-evaluation of self-thinning concepts and status. Ann. Bot. 76, 569–577.
Salo, C., Unnasch, R., Wisnewski, C., 2008. Measuring vegetation with line-point intercept and line intercept methods. Sound Science White Paper Series 3 (www.soundscience.org).
Sherry, T.J., Rowe, C.D., Kirkpatrick, J.D., Brodsky, E.E., 2012. Emplacement and dewatering of the world's largest exposed sand injectite complex. Geochem. Geophys. Geosyst. 13 (8). http://dx.doi.org/10.1029/2012GC004157.
Tabor, N.J., Montañez, I.P., 2002. Shifts in late Paleozoic atmospheric circulation over western equatorial Pangea: insights from pedogenic mineral $\delta^{18}O$ compositions. Geology 30, 1127–1130.
Tabor, N.J., Montañez, I.P., Scotese, C.R., Poulsen, C.J., Mack, G.H., 2008. Paleosol archives of environmental and climatic history in paleotropical western Pangea during the latest Pennsylvanian through Early Permian. Geol. Soc. Am. Spec. Pap. 441, 291–303.
Thomas, B.A., 2013. *In situ* stems: preservation states and growth habits of the Pennsylvanian (Carboniferous) calamitaleans based upon new studies of *Calamites* Sternberg, 1820 in the Duckmantian at Brymbo, North Wales, UK. Palaeontology 57, 21–36.
Tidwell, W.D., 1975. Common fossil plants of western North America. Brigham Young University Press, Provo, Utah (197 pp.).
Tilman, D., 1988. Plant strategies and the dynamics and structure of plant communities. Princeton University Press Monographs in Population Biology 26 pp. 1–360.
Turner, M.G., Gardner, R.H., O'Neill, R.V., 2001. Landscape ecology in theory and practice: pattern and process. Springer, New York (405 pp.).
Wang, J., Pfefferkorn, H.W., Zhang, Y., Feng, Z., 2012. Permian vegetational Pompeii from Inner Mongolia and its implications for landscape paleoecology and paleobiogeography of Cathaysia. Proc. Natl. Acad. Sci. 109, 4927–4932.
West, G.B., Enquist, B.J., Brown, J.H., 2009. A general quantitative theory of forest structure and dynamics. Proc. Natl. Acad. Sci. 106, 7040–7045.
White, J., Harper, J.L., 1970. Correlated changes in plant size and number in plant populations. J. Ecol. 58, 467–485.
Williams, C.J., Johnson, A.H., LePage, B.A., Vann, D.R., Sweda, T., 2003a. Reconstruction of tertiary *Metasequoia* forests II. Structure, biomass and productivity of Eocene floodplain forests in the Canadian Arctic. Paleobiology 29, 271–292.
Williams, C.J., Johnson, A.H., LePage, B.A., Vann, D.R., Taylor, K.D., 2003b. Reconstruction of tertiary *Metasequoia* forests I. Test of a method for biomass determination based on stem dimensions. Paleobiology 29, 256–270.
Wing, S.L., Hickey, L.J., Swisher, C.C., 1993. Implications of an exceptional fossil flora for Late Cretaceous vegetation. Nature 363, 342–344.
Yoda, K., Kira, T., Ogawa, H., Hozumi, H., 1963. Self-thinning in overcrowded pure stands under cultivated and natural conditions. J. Biol. Osaka Univ. 14, 107–129.